

1 **Impact of vehicular emissions on the formation of fine particles in the Sao Paulo**
2 **Metropolitan Area: A numerical study with the WRF-Chem model**

3

4 **Angel Vara-Vela¹, M. F. Andrade¹, Prashant Kumar^{2,3}, R. Y. Ynoue¹, and A. G.**
5 **Muñoz^{4,5}**

6

7 ¹Department of Atmospheric Sciences, Institute of Astronomy, Geophysics and
8 Atmospheric Sciences, University of Sao Paulo, Sao Paulo, Brazil

9 ²Department of Civil and Environmental Engineering, Faculty of Engineering and
10 Physical Sciences (FEPS), University of Surrey, Guilford GU2 7XH, United Kingdom

11 ³Environmental Flow (EnFlo) Research Centre, Faculty of Engineering and Physical
12 Sciences, University of Surrey, Guildford GU2 7XH, United Kingdom

13 ⁴International Research Institute for Climate and Society (IRI), The Earth Institute,
14 Columbia University, NY, USA

15 ⁵Centro de Modelado Científico (CMC), Universidad del Zulia, Maracaibo, Venezuela

16

17 Corresponding author: A. V. Vela (angel.vela@iag.usp.br)

18

19 **Abstract**

20 The objective of this work is to evaluate the impact of vehicular emissions on the
21 formation of fine particles (PM_{2.5}; ≤ 2.5 μm in diameter) in the Sao Paulo Metropolitan
22 Area (SPMA) in Brazil, where ethanol is used intensively as a fuel in road vehicles. The
23 Weather Research and Forecasting with Chemistry (WRF-Chem) model, which
24 simulates feedbacks between meteorological variables and chemical species, is used as
25 photochemical modelling tool to describe the physico-chemical processes leading to

26 evolution of number and mass size distribution of particles through gas-to-particle
27 conversion. A vehicular emission model based on statistical information of vehicular
28 activity is applied to simulate vehicular emissions over the studied area. The simulation
29 has been performed for a one month period (7 August - 6 September 2012) to cover the
30 availability of experimental data from the NUANCE-SPS (Narrowing the Uncertainties
31 on Aerosol and Climate Changes in Sao Paulo State) project that aims to characterize
32 emissions of atmospheric aerosols in the SPMA. The availability of experimental
33 measurements of atmospheric aerosols and the application of the WRF-Chem model
34 made it possible to represent some of the most important properties of fine particles in
35 the SPMA such as the mass size distribution and chemical composition, besides
36 allowing us to evaluate its formation potential through the gas-to-particle conversion
37 processes. Results show that the emission of primary gases, mostly from vehicles, led to
38 a production of secondary particles between 20 and 30 % in relation to the total mass
39 concentration of $PM_{2.5}$ in the downtown SPMA. Each of $PM_{2.5}$ and primary natural
40 aerosol (dust and sea salt) contributed with 40-50% of the total PM_{10} (i.e. those $\leq 10 \mu m$
41 in diameter) concentration. Over 40% of the formation of fine particles, by mass, was
42 due to the emission of hydrocarbons, mainly aromatics. Furthermore, an increase in the
43 number of small particles impaired the ultraviolet radiation and induced a decrease in
44 ozone formation. The ground level O_3 concentration decreased by about 2% when the
45 aerosol-radiation feedback is taken into account.

46

47 **1. Introduction**

48 The Sao Paulo Metropolitan Area (SPMA), in the southeast region of Brazil, is
49 considered a megalopolis comprised of Sao Paulo city and more 38 municipalities. One
50 of the main concern in the SPMA is the occurrence of violations of air quality standards

51 for ozone and fine particles at different air quality stations from the Sao Paulo
52 Environmental Agency (CETESB). The air pollutant emissions in the SPMA are related
53 to the burning of the fuels: ethanol, gasohol (gasoline with 25% ethanol) and diesel.
54 Recent work of Carvalho et al. (2014) reported a substantial increase in number of road
55 vehicles from 1 million in 2000 to almost 7 million in 2014, together with an overview
56 of the pollutants concentration, fuel use in the SPMA and the relationship between the
57 emissions and the improvement in the air quality in past years.

58 They constitute the main cause of impairment to air quality in the SPMA, but
59 the number of air quality standard violations has decreased for almost all pollutants with
60 the exception of PM_{2.5} and O₃. Both these pollutants are impacted by the vehicular
61 emissions and have experienced an increase in the number of violations of local air
62 quality standards as discussed in detail by Carvalho et al. (2014). Pérez-Martínez et al.
63 (2015) have analyzed the monthly mean values for the regulated pollutants from 2000 to
64 2013 for the air quality stations in the SPMA. They found a decrease in the average
65 concentration of NO_x, CO and PM₁₀ by 0.65, 0.37 and 0.71 % month⁻¹, respectively,
66 although the sales of the fuels (gasoline, ethanol, and diesel) had increased by 0.26, 1.96
67 and 0.38 % month⁻¹, respectively.

68 A recent report from CETESB (CETESB, 2013) highlighted that, in 2012, the
69 vehicles contributed with about 40% of the total PM₁₀ mass concentrations through
70 direct emissions. If we consider the secondary aerosols, which were about 25% of PM₁₀
71 as estimated by CETESB (2013), these were mainly found to be formed by chemical
72 reactions between gases released from exhaust of vehicles.

73 The implementation of the Program for the Control of Vehicular Emission
74 (PROCONVE) established by the Brazilian Government in the 80's, enforcing measures
75 such as use of catalytic converters and ethanol as additive to gasoline in substitution of

76 tetraethyllead, led to decrease in emissions of CO and VOCs and hence their ambient
77 concentration. Although the emissions have been controlled by regulations, the number
78 of vehicles has increased substantially and faster than the replacement of the old
79 vehicles by the new ones (Pérez-Martínez et al., 2014). According to CETESB (2013),
80 the road vehicles contributed up to about 97, 87 and 80% of CO, VOCs and NO_x
81 emissions in 2012, respectively, being most of NO_x associated to diesel combustion and
82 most of CO and VOCs from gasohol and ethanol combustion. Receptor modelling
83 studies applied to six capital cities in Brazil (Andrade et al., 2012) showed that only
84 13% of PM_{2.5} in the SPMA is associated to the emission by the industrial processes (oil
85 burning and secondary aerosols).

86 To date, many studies assessing the impact of biofuels on the air quality have
87 been performed in Brazil. For example, Anderson (2009) conducted a review
88 concerning the use of ethanol fuel in Brazil. His work highlighted that the atmospheric
89 concentrations of acetaldehyde and ethanol are much higher in Brazil in comparison
90 with the other areas of the world. Costa and Sodré (2010) showed that exhaust
91 emissions of hydrous ethanol reduced CO and Hydrocarbons (HC), but increased CO₂
92 and NO_x levels.

93 A number of past studies has shown the significant participation of the
94 carbonaceous compounds in the concentration of fine particles in the SPMA
95 (Albuquerque et al., 2011; Miranda and Andrade, 2005; Ynoue and Andrade, 2004;
96 Castanho and Artaxo, 2001). Studies conducted on ambient air pollution in the SPMA
97 have also shown that BC explains 21% of mass concentrations of fine particles (PM_{2.5};
98 $\leq 2.5 \mu\text{m}$ in diameter) compared with 40% of organic carbon (OC), 20% of sulfates, and
99 12% of soil dust (Andrade et al., 2012). Most of the observed ambient PM_{2.5} mass
100 concentration usually originates from precursors gases such as sulphur dioxide (SO₂),

101 ammonia (NH₃), nitrogen oxides (NO_x) and volatile organic compounds (VOCs) as
102 well as through the physico-chemical processes such as the oxidation of low volatile
103 hydrocarbons noted above transferring to the condensed phase (McMurry et al., 2004;
104 Heal et al., 2012). Since these processes are often photo-chemically driven, the resultant
105 aerosol usually falls into the category of secondary photochemical pollutant (Jenkin and
106 Clemitshaw, 2000). Oxidation of VOCs can produce species of sufficiently low vapor
107 pressure to be condensable, leading to the formation of secondary organic aerosol
108 (SOA) (Kroll and Seinfeld, 2008). Fine particles in SPMA have a great participation on
109 its composition of SOA, formed from the emissions of VOCs, which have the same
110 origin of the primary compounds involved in the formation of ozone, from the burning
111 of fuels. The participation of the biogenic emission is considered to be small in the
112 formation of particles in the metropolitan area of the city according to previous studies
113 of Martins et al. (2006).

114 The impact of the fine particles has been discussed in previous works, with
115 evaluation of the scattering and absorbing effects of the aerosol (e.g. Li et al., 2005;
116 Real et al., 2011). Vehicular emissions of particulate matter (PM) in the SPMA have a
117 high percentage of BC (Brito et al., 2013), which after emitted to the atmosphere can
118 enhance the absorption coefficient and thus the attenuation rates.

119 One of the most important aspects of this work is the quantitative analysis of the
120 formation of PM_{2.5} and ozone (O₃) in the SPMA. Photolysis of O₃ by ultraviolet light in
121 the presence of water vapor is the main source of hydroxyl radical (OH), the most
122 important radical in the atmosphere in terms of reactivity (Monks, 2004). At the same
123 time, OH levels in the atmosphere directly determine the oxidation rate of the precursors
124 of secondary aerosols. Oxidation products of VOCs and semi-VOCs by OH are the
125 most important precursors of SOA (Li et al., 2011a). Although VOCs and NO_x are

126 precursors of both O₃ and a fraction of atmospheric PM (NO₃⁻ and secondary organics)
127 while they influence indirectly the formation of the rest of the secondary PM
128 components like SO₄⁼, their control strategies that are optimal for O₃ controls may even
129 increase PM_{2.5} concentrations (McMurry et al., 2004). Such an analysis is important to
130 evaluate the contribution of the vehicular fleet using different kind of fuels to the
131 concentration of fine particles. In this sense, a numerical study with an adequate
132 physical approach, representing particles in the modelling system, is important to
133 understand the formation of secondary aerosols from primary emission of gases in a
134 metropolitan area where the composition of fuel in vehicular fleet has changed
135 significantly over the past years. Therefore, the goal of the present study is to evaluate
136 the impact of vehicular emissions on the formation of fine particles in the SPMA,
137 focusing especially on the potential formation of secondary particles from the primary
138 emission of gases coming from on-road vehicles. The impact of aerosol particles on the
139 ozone photochemistry is also examined by means of numerical simulations.

140 Measurements were performed to provide input data to evaluate the modelling
141 performance and estimate the vehicular emission factors. Aerosol measurements were
142 taken from field campaigns that were carried out as part of the Narrowing the
143 Uncertainties on Aerosol and Climate Changes in Sao Paulo State (NUANCE-SPS)
144 project (<http://nuance-lapat.iag.usp.br/>). These campaigns took place between July and
145 September 2012. An online-coupled meteorology and chemistry model, i.e., the
146 Weather Research and Forecasting with Chemistry (WRF-Chem) model, has been used
147 to characterize and describe the physico-chemical processes involved in both the
148 formation and growth of new particles over the SPMA in southern Brazil. The details of
149 the experimental campaigns, WRF-Chem model and emissions are described in Section

150 2. Results from modelling experiments and comparison with measurements are
151 presented in Section 3. Finally, the summary and conclusions are given in Section 4.

152

153 **2. Methodology**

154 **2.1. Observational datasets**

155 The study period starting from 7 August until 6 September 2012 was selected for
156 comparison with the modelled results (Section 2.2) due to the availability of
157 experimental data from the NUANCE-SPS project. The aim of NUANCE-SPS was to
158 evaluate the impact of emissions in the SPMA on the air quality and changing climatic
159 conditions, and feedback mechanisms between climatic perturbations produced by both
160 primary and secondary emissions and urban atmospheric processes. Aerosol observation
161 datasets used in this work were collected using a Dichotomous sampler (Wedding et al.,
162 1980) and a Micro-Orifice Uniform Deposit Impactor (MOUDI, model 100; MSP
163 Corporation - Marple et al., 1986). The MOUDI impactor collected particles in 10 size
164 classes with nominal 50% cut-off diameters: 10, 5.6, 3.2, 1.8, 1.0, 0.56, 0.32, 0.18, 0.1
165 and 0.06 μm . Particles smaller than 0.06 μm were collected in a subsequent stage or
166 after-filter. The samples collected with the MOUDI impactor were deposited on a
167 polycarbonate membrane filter with 0.4 μm porous and for the Dichotomous sampler
168 the substrate was a teflon membrane filter with 2 μm porous. The after-filter in the
169 MOUDI impactor is a 33 mm teflon membrane filter, which was not submitted to the
170 reflectance analysis. The collected membrane filters sampled with the Dichotomous and
171 MOUDI samplers were analyzed to the identification of trace elements of mass through
172 X-ray diffraction analysis, mass concentration through gravimetric analysis, and black
173 and organic carbon through reflectance and thermo analysis using a thermal-optical
174 transmittance (TOT) (Sunset Laboratory Inc. – Birch and Cary, 1996). Ion

175 concentrations were evaluated through the ion chromatography analysis of the soluble
176 material collected on the membrane filters (sulphate, nitrate, ammonium, sodium, and
177 chloride). All these samplings were performed on the roof of the main building of the
178 Institute of Astronomy, Geophysics and Atmospheric Sciences of the University of Sao
179 Paulo (IAG-USP) (hereafter also referred as IAG-USP measurement site or simply
180 IAG-USP), which is inside a small green-park (approximately 7.4 km²), with local
181 traffic during the day and surrounded by major roads with intense traffic by light and
182 heavy-duty vehicles (Nogueira et al., 2014). Table 1 lists the aerosol instrumentation
183 deployed roughly at the IAG-USP measurement site. In addition, ambient data from the
184 CETESB's air quality monitoring network and the IAG-USP's climatological station
185 (hereafter also referred as AF-IAG) were also considered for evaluation of numerical
186 simulations. The locations of measurement sites are depicted in Fig. 1 whereas
187 geographic coordinates, urban-suburban classification, and the list of pollutants and
188 meteorological parameters monitored at each site is available in Table 2.

189

190 **2.2. WRF-Chem model**

191 The WRF-Chem model is a fully coupled online meteorological and chemical
192 transport model (Grell et al., 2005), supported by National Center for Atmospheric
193 Research (NCAR) of the USA and several other research institutions around the world.
194 This model is a system of two key components. The WRF-Chem meteorological
195 component, the Weather Research and Forecasting (WRF), is a system configured for
196 both research and operational applications. The dynamical core used in this study is the
197 Advanced Research WRF (ARW). Model's equations into ARW are solved to non-
198 hydrostatic conditions on a fully compressible atmosphere. Further details on the
199 modelling system can be found on the WRF model website (<http://www.wrf->

200 model.org). On the other hand, the WRF-Chem chemical component treats chemical
201 processes such as dry deposition, gas-phase chemistry, photolysis rates, and aerosols
202 chemistry. A detailed description of the WRF-Chem model can be found on its website
203 (<http://ruc.noaa.gov/wrf/WG11>). Since both meteorological and chemical components
204 are fully coupled, the transport of all chemical species is on-line. The gas-phase
205 chemistry and aerosol modules employed in this study are the Regional Acid Deposition
206 Model, version 2 (RADM2) (Chang et al., 1989) and the Modal Aerosol Dynamics
207 Model for Europe - Secondary Organic Aerosol Model (MADE - SORGAM)
208 (Ackermann et al., 1998; Schell et al., 2001), respectively. The inorganic species
209 included in the RADM2 mechanism are 14 stable species, 4 reactive intermediates, and
210 3 abundant stable species (oxygen, nitrogen and water). Atmospheric organic chemistry
211 is represented by 26 stable species and 16 peroxy radicals. The RADM2 mechanism
212 represents organic chemistry through a reactivity aggregated molecular approach
213 (Middleton et al., 1990). Similar organic compounds are grouped together in a limited
214 number of model groups through the use of reactivity weighting. The aggregation
215 factors for the most emitted VOCs are given in Middleton et al. (1990).

216 On the other hand, the most important process for the formation of secondary
217 aerosol particles is the homogeneous nucleation in the sulfuric acid-water system. It is
218 parameterized in MADE, following the method of Kulmala et al. (1998). Aerosol
219 growth by condensation occurs in two steps: the production of condensable material
220 (vapor) by the reaction of chemical precursors, and the condensation and evaporation of
221 ambient volatile species on aerosols. The inorganic chemistry system, based on the
222 Model for an Aerosol Reacting System (MARS) (Saxena et al., 1986) and its
223 modifications by Binkowski and Shankar (1995), calculates the chemical composition
224 of a sulphate-nitrate-ammonium-water aerosol according to equilibrium

225 thermodynamics. The organic aerosol chemistry is based on the SORGAM, which
226 assumes that SOA compounds interact and form a quasi-ideal solution (Grell et al.,
227 2005). The SOA formation in SORGAM follows the two-product approach (Odum et
228 al., 1996) where the oxidation of hydrocarbons produces two types of modelled
229 semivolatile compounds that are partitioned between the gas and particle phases after
230 considering the absorptive partitioning theory (Pankow, 1994a; b). The primary organic
231 aerosol (POA) in MADE is calculated from the primary anthropogenic emission of OC.
232 Then, one may calculate the predicted OC concentration from the sum of both SOA and
233 POA. The concurrent organic matter (OM) can be obtained from the OC concentration
234 by application of a conversion factor. Brown et al. (2013) showed that the average
235 OM:OC ratio was 1.54 (with a standard deviation of 0.2) for sites with low amount of
236 secondary aerosol formation. It is important to note that this ratio can change from one
237 place to another. In areas impacted by biomass burning the ratio can be higher. Gorin et
238 al. (2006) assumed a ratio of 1.6 for the conversion from OC to OM over an area that
239 experiences a significant wood smoke influence.

240

241 **2.2.1. Model configuration**

242 WRF-Chem version 3.5 was configured with three nested grid cells: coarse (75
243 km), intermediate (15 km) and fine (3 km). The coarse grid cell covered a big region of
244 Brazil and also of the Atlantic Ocean. The intermediate grid covered the southeast
245 Brazil while the fine grid cell covered barely the SPMA and metropolitan areas nearest
246 to it. Fig. 1 shows the arrangement of measurement sites and topography in the
247 downtown area of the 3-km modelling domain. The initial and boundary meteorological
248 conditions are from the National Center for Environmental Prediction's Final
249 Operational Global Analysis with 1° of grid spacing, 26 vertical levels and are available

250 every six hours: 00, 06, 12 and 18 UTC (<http://rda.ucar.edu/datasets/ds083.2/>). The
251 initial and boundary chemical conditions for representing gases and aerosols
252 background concentration were obtained from the Model for Ozone and Related
253 chemical Tracers, version 4 (MOZART-4; Emmons et al., 2010). This model was
254 driven by meteorological inputs from the Goddard Earth Observing System Model,
255 version 5 at a horizontal resolution of $1.9^{\circ} \times 2.5^{\circ}$, 56 vertical levels that are also available
256 every six hours. Table 3 lists the WRF-Chem configuration options employed by this
257 study.

258 WRF-Chem simulation with coupled primary aerosol (dust, sea salt and
259 anthropogenic) and gas (biogenic and anthropogenic) emission modules, together with
260 the direct effect of aerosol particles turned on, is performed as the control simulation in
261 order to evaluate the model performance (hereafter referred to as Case_0). For
262 secondary aerosols, a simulation scenario (Case_1) with biogenic and anthropogenic
263 gases emission is performed to evaluate its formation potential. An additional
264 simulation (Case_2) is also performed to evaluate the impact of aerosols on ozone
265 photochemistry. Notation and description of simulations are listed in Table 4. The first
266 seven days of each simulation were not analyzed and used for model spin-up.

267

268 **2.3. Emissions**

269 **2.3.1. Anthropogenic emissions**

270 Because on-road vehicles are the most important sources of air pollution in
271 southeast Brazil's metropolitan areas, particularly in SPMA where, according to
272 CETESB, more than 80% of pollutant emissions are generated by vehicular emissions;
273 the anthropogenic emissions of trace gases and particles in both 3 and 15 km modelling
274 domains were considered to include emissions only coming from on-road vehicles

275 through the use of a vehicular emission model developed by the IAG-USP's Laboratory
276 of Atmospheric Processes (LAPAt). Basically, this model considers the number of
277 vehicles, vehicular emission factors, and average driving kilometers for vehicle per day
278 as basic parameters for the calculation of exhaust emissions considering different
279 vehicle types (light-duty vehicles, heavy-duty vehicles, and motorcycles) and different
280 fuel types (ethanol, gasohol, combination of any proportion of gasohol and ethanol, and
281 diesel) according to CETESB (2012). The details of this model are available in Andrade
282 et al. (2015). In the case of VOCs, there are other two relevant emissions (fuel transfer
283 and evaporative processes) associated with the vehicles, besides the exhaust emissions.
284 Because of the complexities in the spatial representation due to a numerous factors such
285 as emissions at service stations, such emission sources are assumed to be emitted by
286 exhaust of vehicles for the sake of simplicity. The vehicular fleet and intensity of use
287 datasets are provided by the National Department of Traffic (DENATRAN) and the Sao
288 Paulo Transporte (SPTrans), respectively. Emission factors for road vehicles for most
289 pollutants were considered from previous studies performed inside road tunnels (i.e.
290 Janio Quadros, referred as JQ tunnel, and the tunnel 3 of the Rodoanel Mario Covas that
291 is referred hereafter as RA tunnel) located within the SPMA (Pérez-Martínez et al.,
292 2014; Nogueira et al., 2014). However, emission factors for VOCs are considered from
293 dynamometer protocols (CETESB, 2010). VOCs and PM speciation profiles used by
294 gas-phase and aerosol chemical modules were also obtained from NUANCE-SPS
295 experimental campaigns performed in 2011 (tunnel measurements) and 2012 (ambient
296 data). It is important to note that due to the lack of information on vehicular emission
297 factors and intensity of use for most of the other metropolitan areas inside both
298 modelling domains (e.g. the Campinas Metropolitan Area, which is shown by the
299 second largest grey stain in Fig. 2), the calculation of vehicular emissions for these

300 urban areas was carried out on the basis of the parameters found for the SPMA. The
301 number of vehicles in any modelling domain is calculated from the sum of the number
302 of vehicles in each one of the main urban areas inside the modelling domain in question.

303 Spatial distribution of emissions for the 3 km modelling domain resolution was
304 based on road density products compiled by the OpenStreetMap project and extracted
305 from the Geofabrik's free download server (<http://download.geofabrik.de>). Urban areas
306 were assumed to allocate high emissions since these concentrate a road density greater
307 than other areas. In the case of the 15 km modelling domain, emissions are based on
308 night-time lights data from the Defense Meteorological Satellite Program
309 (<http://ngdc.noaa.gov/eog/dmsp/downloadV4composites.html>). These images are 30 arc
310 second grids, spanning from -180° to $+180^{\circ}$ longitude and -65° to $+75^{\circ}$ latitude and
311 contain the lights from cities, towns and other sites with persistent lighting, including
312 gas flares. Cleaned up night-time light points with no ephemeral events such as forest
313 fires are used to allocate emissions. To estimate the number of vehicles in each grid
314 point of both domains, the sum of individual intensities at each point (i.e. total road
315 length for the 3 km modelling domain and night-time light for the 15 km modelling
316 domain) is firstly normalized by the total fleet, and then distributed uniformly using the
317 total fleet distribution so that emissions in urban areas are mainly represented by
318 emissions coming from their vehicles. Furthermore, due to the complexity involved in
319 describing the temporal variation of emissions at each grid point, median values for
320 vehicular traffic obtained from measurements inside the JQ and RA tunnels (Pérez-
321 Martínez et al., 2014) were used for distributing the emissions during the day in both
322 domains. This approximation followed the approach used by Fast et al. (2006) where
323 emission profiles were calculated from median diurnal variations on weekdays and
324 weekends. We have applied the same constant diurnal cycle at all grid points where

325 emissions have values greater than zero. VOC and PM emission profiles were assumed
326 to be the same as for CO and NO_x emission profiles since these pollutants are also
327 characteristic tracers of emissions of light-duty and heavy-duty vehicles, respectively.
328 Fig. 2 shows the maximum hourly emission rates for aromatic VOCs in the 3 km
329 modelling domain. Anthropogenic emissions were not considered in the 75 km
330 modelling domain.

331 The Another Assimilation System for WRF-Chem (AAS4WRF) chemical
332 emissions pre-processor developed by the Latin American Observatory (OLE2; Muñoz
333 et al., 2010; 2012) was used to scale emission rates on WRF curvilinear coordinates.
334 AAS4WRF is appropriate to write chemical emission rates from both surface and
335 elevated sources in the proper WRF data file format, providing an alternative tailored
336 way to assimilate emissions to WRF-Chem. The method is explained in the OLE2 Wiki
337 pages in detail (http://www.cmc.org.ve/mediawiki/index.php?title=Calidad_de_Aire).

338

339 **2.3.2. Other emissions**

340 Biogenic emissions are calculated online based on the Guenther scheme
341 (Guenther et al., 1993; 1994). The Guenther biogenic emissions model calculates the
342 emission rates using temperature, photo-synthetically active radiation flux and land-use
343 data as the U.S. Geological Survey (USGS) land-use cover system classification if
344 coupled with the WRF model. However, as indicated in the WRF-Chem emissions
345 guide (http://ruc.noaa.gov/wrf/WG11/Emission_guide.pdf), several key chemical
346 species would have been representing relatively low emission rates because of the
347 limited vegetation types in the simulation, and thus their impacts are anticipated to be
348 much lower than those from vehicular emissions.

349 Dust and sea salt emissions are calculated online following the works of Ginoux
350 et al. (2001) and Gong (2003), respectively. The calculation of Ginoux et al. (2001) for
351 the uplifting of dust particles is based on the surface wind speed, wetness and
352 information on soil characteristics. The model then solves the continuity equation
353 including the emission, chemistry, advection, convection, diffusion, dry deposition, and
354 wet deposition of each species. The parameterization of sea salt aerosol source function
355 of Gong (2003) is an extended parameterization of Monahan et al. (1986), which scales
356 the generation of marine aerosols from mechanical disruption of wave crests by the
357 wind and sea surface covered by whitecaps.

358

359 **3. Results and discussion**

360 **3.1. Characterization of meteorological conditions**

361 In order to study and understand the spatial and temporal variability of
362 atmospheric aerosols, O₃, and other pollutants (i.e. CO, NO_x) during the study period, it
363 was first necessary to analyze the behavior of main meteorological systems acting on
364 the atmospheric environment of the SPMA and surrounding areas.

365 According to the monthly climate reports from the IAG-USP's Climate Research
366 Group (GrEC), the observed precipitation rates were lower than the climatological value
367 in SPMA (anomaly of -38.6 mm) and larger part of the Sao Paulo State during August
368 2012. Negative anomalies on the precipitation were caused by the intensification of the
369 South Atlantic Subtropical High (SASH). These conditions established an easterly wind
370 anomaly pattern at the 850 hPa level. Conditions were unfavorable for relative humidity
371 coming from the Amazon due to the Low Level Jet (LLJ) and less intense Alisian winds
372 in the Tropical Atlantic (GrEC, 2012a). However, the action of frontal systems favored
373 the rain accumulation in September 2012, mainly in western Sao Paulo State where the

374 greater positive amount of anomalies was observed. Precipitation events were
375 predominantly observed during the second half of the month. In this case, the wind
376 pattern showed an opposite configuration to that observed in August 2012 as a result of
377 the weakening of the SASH (GrEC, 2012b). The IAG-USP's climatological station
378 recorded an accumulated precipitation of about 1.3 mm on three days of occurrence (28
379 August, 30 August and 4 September 2012) and an easterly wind pattern with a median
380 intensity of 2 m s^{-1} during the period between 07 August and 06 September 2012. Fig. 3
381 shows the hourly accumulated precipitation and relative humidity observed at the IAG-
382 USP's climatological station.

383

384 **3.2. Analysis of aerosol species**

385 Aerosol analysis included species such as organic carbon (OC), elemental
386 carbon (EC), sulphate, nitrate, ammonium, sodium and chloride in addition to other
387 elemental constituent of PM. All the samplings for these species were performed at
388 IAG-USP. Results showed that the major contributors to the concentration of fine
389 particles are OM (55.7%; OM:OC ratio of 1.5 found by Brito et al. (2013)) and EC
390 (15%), followed by sulphate (2.9%), ammonium (2.1%), sodium (1.9%), nitrate (0.5%)
391 and chloride (0.3%). The remaining mass (21.6%) is calculated by determining of the
392 difference between the total mass of $\text{PM}_{2.5}$ (from the gravimetric analysis) and the sum
393 of the masses of 7 individual compounds, as noted above. Part of this remaining mass is
394 related to the water content of aerosols (Andrade et al., 2012).

395 On the other hand, $\text{PM}_{2.5}$, PM_{10} and size distribution of particles measured at
396 IAG-USP show that the study period was characterized by a reduction in the

397 concentrations up to the end of August 2012 when their minimum values were
398 achieved. This reduction was related to the action of a semi-stationary front between the
399 coasts of Sao Paulo and Parana States. After the passage of this system, aerosol
400 concentrations have significantly increased what could be related to an increase in
401 relative humidity once the SASH system is moved away from the continent, as well as
402 the transport of aerosol particles produced by forest fires in the central-west region of
403 Brazil and the Sao Paulo State. Several studies have shown the contribution of forest
404 fires on the atmospheric aerosol concentrations in SPMA (Vieira-Filho et al., 2013;
405 Vasconcellos et al., 2010). One way to qualitatively evaluate the contribution of forest
406 fires on aerosol concentrations is by using the air mass trajectories. The Hybrid Single-
407 Particle Lagrangian Integrated Trajectory (HYSPPLIT) model (Draxler and Hess, 1998)
408 was used to calculate backward trajectories of air masses in order to identify
409 atmospheric transport of air mass from forest fire areas. Fig. 4 shows the three-day
410 backward trajectories of air masses starting at IAG-USP for the days 9 and 31 August
411 and 5 September, when increases in the OC and EC concentrations were observed at
412 IAG-USP. The pink markers on the map represent the observed fire locations during the
413 study period considering different satellite products (GOES, AQUA, TERRA, NOAA).

414 Fig. 5 shows the concentration of OC, EC and some species of PM_{2.5} during the
415 study period at IAG-USP. We can observe eleven exceedances of PM_{2.5} concentration
416 with respect to the air quality standard of 25 $\mu\text{g m}^{-3}$ (see grey line in Fig. 5a) established
417 by the World Health Organization (WHO). These exceedances have mainly occurred at
418 the beginning and at the end of the study period when an increase in the concentrations
419 of OC and EC were observed. The increasing organic matter could be associated to
420 traffic incidents which may raise the emissions, which in case of less favorable
421 meteorological conditions (e.g. lower height of lower planetary boundary layer, PBL, or

422 slow transport of air pollutants) may have led to a more efficient formation of secondary
423 particles. Castanho and Artaxo (2001) analyzed the behavior of the aerosol composition
424 in SPMA and showed the increase in the concentration of inorganic and organic
425 material in the winter season compared to the summer season, explaining this behavior
426 with the meteorological characteristics: dry conditions with low height inversion layer
427 in the wintertime and a rainy summer.

428 Size distributions of aerosol mass indicate that the majority of sulphate,
429 ammonium and PM_{10} mass concentration is distributed in the size range with diameters
430 between 0.1 and 1 μm , commonly known as accumulation mode particles (Kumar et al.,
431 2010). In the cases of nitrate, sodium, and chloride, most part of mass was concentrated
432 in particles with diameters greater than 1 μm .

433

434 **3.3. Comparison of baseline simulation with observations**

435 All the numerical results presented in this section, for the purpose of comparison
436 with the measurements, were obtained from the baseline simulation (Case_0). The
437 predicted temperature, humidity, and 10-m wind speed and direction have been
438 compared to measurements from the AF-IAG and INT measurement sites. Overall, the
439 model captured the diurnal variation of temperature, relative humidity, and wind
440 directions reasonably well. However, the predicted wind speeds were higher than the
441 observed values. To evaluate the model performance in solving the meteorology and
442 chemical species, we computed the statistics correlation coefficient (R), mean bias
443 (MB), mean fractional bias (MFB), mean fractional error (MFE), and root mean square
444 error UB ($RMSE_{UB}$). The definitions of these statistics are given in the Appendix. Fig. 6
445 shows the predicted average of 10-m wind vectors and 2-m temperature for the whole
446 study period in the 3 km modelling domain. Blue dots represent the locations of AF-

447 IAG and INT sites, while the numbers in cyan indicate the observed average
448 temperatures (i.e. 17.7 °C at AF-IAG and 17.8 °C at INT). On an average, the predicted
449 wind direction was easterly in SPMA, which has somewhat affected the spatial
450 distribution of aerosol particles as examined later in this section. Likewise, the statistics
451 used to quantify the model performance in the representation of PM concentration show
452 that, in general, most of prediction-observation pairs present good correlation
453 coefficients, mainly those for PM₁₀, but with negative biases and standard deviations
454 lower than those for observations (see Fig. 10). Table 5 summarizes the performance
455 statistics used in this study showing comparisons between WRF-Chem predictions and
456 observations. The evaluation of WRF-Chem predictions for meteorology and chemical
457 species on a site-by-site basis is presented in the sections 1 and 2, respectively, of the
458 supplementary material. Figs. 7, 8 and 9 show the observed and predicted temporal
459 variations of PM_{2.5}, PM₁₀ and O₃ concentrations at 3, 10 and 6 sites in the SPMA,
460 respectively, with some measurement sites sharing the same grid point for comparisons
461 due to the geographical proximity (e.g. the sites IAG-USP and IPEN-USP both
462 separated around 900 m from each other). These figures suggest that predicted
463 concentrations did not present any significant spatial variation in the downtown SPMA
464 and were generally underestimated when compared to measurements. This under
465 prediction could be associated with an underestimation on the vehicular emissions as
466 well as other emission sources (e.g. emissions coming from industry) that are
467 disregarded in this study, in addition to predicted surface winds more intense than those
468 observed, leading to a dilution of aerosol particles in the SPMA. The high
469 concentrations of PM_{2.5} and PM₁₀ observed at the beginning and at the end of the study
470 period, whose variability and trends were reasonably well captured by the model, could
471 be related with the emission of high aerosol loadings due to traffic incidents as well as

472 the establishment of lower PBL heights, commonly observed under post-frontal
473 situations. The results for this simulation (Case_0) show that overall the predicted PBL
474 heights (not shown here) have a regular diurnal variation in the downtown SPMA with
475 averaged daily values around 500 m at both the beginning and the end, and of up to 700
476 m in the middle of the study period, when lower concentrations of aerosols were
477 observed.

478 Figures 11-13 show the predicted average surface distribution of $PM_{2.5}$, PM_{10}
479 and $PM_{2.5}:PM_{10}$ ratio for the 3 km modelling domain, respectively. Red dots and cyan
480 numbers represent the locations and the observed mean PM concentrations (or mean
481 PM concentration ratios) at the measurement sites, respectively. Major contributions of
482 $PM_{2.5}$ on the total PM_{10} concentration were observed mainly over offshore continental
483 areas (see Fig. 13). High $PM_{2.5}:PM_{10}$ concentration ratios would be firstly associated
484 with the transportation of fine particles and gases from upwind regions (see Fig. 6),
485 followed by a production of fine particles from biogenic emissions. Additional
486 comparisons between the observed and predicted concentrations of OC and EC at IAG-
487 USP (the only site with measurements of OC and EC) are shown in Fig. 14. As it has
488 been pointed out in the section 2 of the supplementary material, under predicted OC
489 concentrations could be associated, among others (e.g., underestimation of POA
490 emissions, inaccurate meteorological predictions), with an underestimation of SOA,
491 probably due to the absence of oxidation of monoterpenes and a limited treatment of
492 anthropogenic VOCs oxidation in the RADM2 mechanism, as discussed by Tuccella et
493 al. (2012). The SORGAM aerosol module considers the formation of anthropogenic
494 SOAs from the oxidation of alkane, alkene and aromatic VOCs as well as the biogenic
495 SOA formation from the oxidation of alpha-pinene, limonene and isoprene VOCs.
496 Recent studies coupling non-traditional SOA models (volatility basis set approaches) in

497 WRF-Chem show improvements in the predicted SOA concentrations, although these
498 are still lower than those observed (e.g. Li et al., 2011b; Ahmadov et al., 2012;
499 Shrivastava et al., 2013).

500 On the other hand, measurements of mass size distribution were also made with
501 a MOUDI impactor at IAG-USP, following the protocol describe in Miranda and
502 Andrade (2005). Constituents of aerosol were subsequently determined by X-Ray
503 fluorescence analysis and ion chromatography analysis. As previously indicated in this
504 section, the main identified species are SO₄, NO₃, NH₄, Na and Cl. The observed
505 average aerosol composition is derived using measurements from both MOUDI
506 impactor and SUNSET analyzer. To perform the comparisons of mass size distribution,
507 we adequately joined the MOUDI bin sizes according to the three modes used by the
508 MADE aerosol module: Aitken (<0.1 μm), accumulation (0.1-1 μm) and coarse (>1
509 μm). The observed and predicted aerosol mass size distributions averaged over the same
510 sampling time period (16 days along the study period) are shown in Fig. 15. Over the
511 downtown SPMA, both the observed and predicted fine particles from accumulation
512 mode account for majority of the total PM_{2.5} mass. Since the formation-growth
513 processes of aerosols in question are explicitly treated in the Aitken and accumulation
514 modes, the predicted concentrations for particles larger than 1 μm are assumed to be
515 zero. In this case, the mass of particles larger than 1 μm is allocated to the PM₁₀ aerosol
516 variable (see Fig. 15). The comparison between the observed and predicted average
517 contributions for the main identified aerosol constituents at IAG-USP is shown in Fig.
518 16. Both the observed and predicted OC and EC make up the largest fraction of PM_{2.5}
519 mass with contributions of 55 and 40%, respectively. In addition, it was found that the
520 predicted SOA concentrations contribute 17% of the predicted total OC concentration at
521 this measurement site. Various global and regional scale SOA simulations have been

522 conducted using mass-based yield and partitioning coefficients, but they have
523 underestimated the SOA concentrations by roughly an order of magnitude, especially
524 over urban regions (Matsui et al., 2014). Using the same SOA formation approach
525 employed by this study and a conversion factor of 1.6 to convert the emissions of OC to
526 OM, Tuccella et al. (2012) found simulated SOA:OM ratios in the 5-40% range against
527 the observed range of 50-80%. Although the predicted average PM_{2.5} concentration
528 (14.48 μg m⁻³) was lower than observed (22.32 μg m⁻³), the mean aerosol chemical
529 composition was reasonably well represented by the model (see Fig. 16).

530 **3.4. Contribution of dust-sea salt and coarse anthropogenic aerosols to PM** 531 **concentration**

532 The evaluation of the contribution of dust and sea salt aerosols on PM₁₀
533 concentration is performed from the sum of their concentrations divided by the PM₁₀
534 concentration. The simulated average ratio between dust–sea salt aerosols and the total
535 PM₁₀ mass concentration is shown in Fig. 17b. High concentration ratios have been
536 observed over the ocean where sea salt emissions are by far the most important aerosols
537 source. Unlike high concentration ratios over the ocean, lower concentration ratios are
538 observed over the continent far away from the coast. In this region, the main sources of
539 atmospheric aerosols would be the emission of primary biological aerosol, SOA formed
540 from the emission of biogenic volatile organic compounds (BVOCs), and forest fires.
541 However, particles could also be transported from remote areas. In addition, we can also
542 observe that dust and sea salt aerosols have a contribution between 40 and 50% of the
543 total PM₁₀ concentration in the downtown SPMA. Furthermore, it is possible to estimate
544 the contribution of all the other PM₁₀ (i.e., the coarse anthropogenic aerosol) to the total
545 PM₁₀ mass concentration. It may be directly calculated from the model or estimated
546 from the Figs. 13 and 17b once the sum of concentrations of PM_{2.5}, dust and sea salt,

547 and coarse anthropogenic aerosol represents 100% of the total PM_{10} mass concentration.
548 For example, we found that the coarse anthropogenic aerosol represents around 10% of
549 PM_{10} in the downtown SPMA.

550 **3.5. Evaluation of secondary aerosol formation**

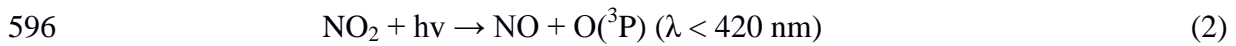
551 As described in Section 2.1, aerosol module employed by this study
552 (MADE/SORGAM) includes the homogeneous nucleation in the sulphuric acid-water
553 system. The sulphuric acid is the most significant condensable molecule formed in the
554 atmosphere, which has also been long recognised as the most important molecule from
555 the point of view of the nucleation of new particles (Jenkin and Clemitshaw, 2000;
556 Seinfeld and Pandis, 2006). However, for the SPMA, the importance of SOA formed
557 from the anthropogenic emission of fuel used by the transport sector was noted (Salvo
558 and Geiger, 2014). According to the official emission inventory developed by the Sao
559 Paulo Environmental Protection Agency (CETESB, 2013), the SOA explains 51% of
560 the fine particle mass concentration, with the vehicular emission being its main source.
561 The subsequent growth processes involve aerosol growth by condensation of
562 condensable material onto existing particles, and by coagulation of particles to form
563 larger particles (Kumar et al., 2011; 2014). For example, particles in the accumulation
564 mode emerge through coagulation of particles from the Aitken mode (Kumar et al.,
565 2011). It is important to emphasize that the boundaries were updated with gas and
566 aerosol background concentrations coming from the 15 km modelling domain during
567 the whole simulation period. Thereafter, the impact of vehicular emissions on the
568 formation of fine particles was calculated from the predicted $PM_{2.5}$ concentration
569 considering an emission scenario (Case_1) in which only emission of gases from
570 vehicles and vegetation are taken into account to be emitted to the atmosphere from the
571 surface. The predicted average $PM_{2.5}$ (Case_1): $PM_{2.5}$ (Case_0) ratio is shown in Fig.

572 17a. A contribution between 20 and 30% in the predicted baseline PM_{2.5} concentration
573 in downtown SPMA is found to correspond to the fine particles formation and
574 transportation processes. Higher concentration ratios over the SPMA surroundings (30-
575 50%) could be associated with more efficient biogenic emissions. Overall, it is observed
576 that the formation efficiency increases towards the northwest from the ocean. Deep red
577 areas in Fig. 17a could also be associated with the transportation of fine particles and
578 gases from other regions, in addition to having a more efficient production of fine
579 particles from biogenic emissions. For example, given the distribution of winds in Fig.
580 6, the northern boundary could represent the main source of particles and gases over this
581 part of the simulation domain. Additionally, the comparison between the predicted and
582 observed OC and EC concentrations at IAG-USP shown in Fig. 14 includes the Case_1
583 simulation in which only emission of primary gases is taken into account in the
584 assessment of fine particles formation. The concentration peaks observed at the
585 beginning and at the end of the study period may be associated with the transport of
586 aerosol particles from both biomass and fossil fuel burning areas (see Fig. 4).
587 Considering the Case_1 simulation, we can observe very low concentrations for EC
588 (mean concentration of 0.01 µg m⁻³), as expected. This is because these particles are not
589 produced by photochemical processes in the atmosphere, but associated mainly with the
590 diesel exhaust.

591 **3.6. Aerosol impact on O₃ photochemistry**

592 Ozone photochemistry production mainly depends on the two key photolysis
593 rates, as shown in Eqs. (1) and (2), i.e., shortwave radiation able to reach the surface to
594 break molecules of O₃ and NO₂.





597 Therefore, the impact of aerosols on O₃ photochemistry has been evaluated from
598 the impact of aerosols on downward shortwave radiation. Attenuation (scattering and
599 absorption) of downward shortwave radiation by aerosols may substantially modify the
600 photolysis rates, and thereby affecting the ozone photochemistry production.

601 The average percentage change in surface O₃ concentrations at 16:00 h (local
602 time) with and without the aerosol-radiation feedback module turned on are shown Fig.
603 17c. Overall O₃ is destroyed or formed (incoming transport from other regions) in small
604 quantities between -1 and +1% in relation to its total concentration. In addition, it was
605 observed that the surface O₃ concentration decreased by around 2% in the downtown
606 SPMA. Li et al. (2011a) found that the impact of aerosols on O₃ formation in Mexico
607 City was most pronounced in the morning with the O₃ reduction of 5-20%, but the
608 reduction is less than 5% in the afternoon. Low reductions in the O₃ concentration in the
609 downtown SPMA compared to results from other studies may be explained by the lower
610 predicted PM₁₀ concentrations, which can lead to a minor attenuation of the incoming
611 solar radiation. Simulated mean downward shortwave fluxes at ground surface (not
612 shown) were up to 5% higher for the Case_2 than for the Case_0 during the afternoon.
613 The inclusion of the direct effect of aerosol particles was found to have small reductions
614 in the surface temperature (changes by around 2%), presumably due to an increase in
615 the number of atmospheric processes involving downward longwave fluxes over this
616 area. Forkel et al. (2012) found an underestimation of predicted downward longwave
617 radiation over the southern Baltic Sea when the direct effect of aerosol particles was
618 neglected. Despite the highly non-linear behavior of tropospheric O₃, the reduction in
619 the predicted O₃ concentrations indicates a high efficiency of aerosols to attenuate the

620 downward shortwave radiation, what is plausible once it was found that low PM_{10}
621 concentrations have a capability to reduce ground level O_3 concentrations in a few ppb.

622 **4. Summary and conclusions**

623 The WRF-Chem community model has been used to evaluate the impact of
624 vehicular emissions on the fine particles formation in the SPMA. Three thirty-one day
625 simulations, covering a period from 7 August to 6 September 2012, have been
626 performed. The aims were to evaluate the impact of fine particles formation (both
627 inorganic and SOA) from gases emitted by road vehicles as well as the aerosol impacts
628 on the ozone formation photochemistry. The results were compared with the
629 measurements available from the NUANCE-SPS project.

630 The predicted temporal variations of meteorology, $PM_{2.5}$, PM_{10} and O_3 were
631 found to agree well with the measurements at most of the sites during the entire
632 simulation period. However, the predicted concentrations of $PM_{2.5}$, PM_{10} and O_3 (but in
633 minor intensity) were lower than the observed values. This difference could be
634 associated with an underestimation of the vehicular emissions and other emission
635 sources such as industry, heating and cooking, which are not considered in this study.
636 Wind speed and direction played an important role in the distribution of fine particles
637 over the simulation domain. Backward trajectories analysis suggested that aerosol
638 particles from biomass burning were transported to SPMA, impacting on the PM
639 concentration over this region.

640 The baseline simulation (Case_0) showed that dust and sea salt aerosols made a
641 contribution between 40 and 50% of the total PM_{10} concentration in the downtown
642 SPMA. On the other hand, the Case_1, which represents simulations with gaseous
643 emissions only, indicates that the emissions of primary gases coming mainly from

644 vehicles have a potential to form new particles between 20 and 30% in relation to the
645 baseline PM_{2.5} concentration found in the downtown SPMA. Finally, the Case_2, which
646 represents simulations with aerosol-radiation feedback turned on, reveals a reduction in
647 the surface O₃ concentration by around 2% in the afternoon (16:00 h; local time) when
648 the aerosol-radiation feedback is taken into account.

649 This study provides a first step to understand the impact of vehicular emissions
650 on the secondary particles formation in the SPMA. Nevertheless, more experimental
651 campaigns are recommended for future work in order to characterize aerosols in
652 ambient air and to improve their emission estimates so that a better understanding of
653 physical and chemical properties and their formation can be established. This study also
654 evaluates the importance of the VOCs in the formation of not only O₃ but also of fine
655 particles. These compounds play an important role concerning health impacts and
656 climate change, and the control of their concentrations requires the description of their
657 formation mechanisms.

658 **Appendix**

659 The statistics used in this study are defined as follows:

- 660 1. Mean bias (MB)

$$MB = \frac{1}{n} \sum_{i=1}^n (M_i - O_i)$$

661

- 662 2. Mean fractional bias (MFB)

$$MFB = \frac{1}{n} \sum_{i=1}^n \frac{2(M_i - O_i)}{M_i + O_i} 100\%$$

663

- 664 3. Mean fractional error (MFE)

$$\text{MFE} = \frac{1}{n} \sum_{i=1}^n \frac{2|M_i - O_i|}{M_i + O_i} 100\%$$

665

666 4. Root mean square error UB (RMSE_{UB})

$$\text{RMSE}_{\text{UB}} = \sqrt{\frac{1}{n} \sum_{i=1}^n [(M_i - \bar{M}) - (O_i - \bar{O})]^2}$$

667

668 5. Correlation coefficient (R)

$$r = \frac{\sum_{i=1}^n (M_i - \bar{M}) * (O_i - \bar{O})}{\sqrt{\sum_{i=1}^n (M_i - \bar{M})^2} \sqrt{\sum_{i=1}^n (O_i - \bar{O})^2}}$$

669

670 Where

671 $\bar{O} = \frac{1}{n} \sum_{i=1}^n O_i$ and $\bar{M} = \frac{1}{n} \sum_{i=1}^n M_i$ are the average values of the individual observed and

672 predicted values, O_i and M_i , respectively. “n” is the number of observations.

673

674 5. Acknowledgments

675 Prashant Kumar, Angel Vara-Vela and Maria de Fatima Andrade thank the

676 University of Surrey's International Relations Office for the Santander Postgraduate

677 Mobility Award that helped Angel Vara to visit University of Surrey, UK, and develop

678 this research article collaboratively. The authors from Universities of Surrey and Sao

679 Paulo also acknowledge the collaborative funding received through the University

680 Global Partnership Network (UGPN) to the project titled “*Emissions And Role Of Fine*

681 *Aerosol Particles In Formation Of Clouds and Precipitation (eRAIN) - A demonstration*

682 *study for the megacity, São Paulo*” for supporting this research work. Maria de Fatima

683 Andrade and Angel Vara-Vela acknowledged funding from the Coordination for the
684 Improvement of Higher Education Personnel (CAPES) and Research Foundation of the
685 State of Sao Paulo (FAPESP, project 2008/58104-8) that allowed the experimental
686 campaigns. The authors also thank the WRF-Chem developers, the NOAA's National
687 Geophysical Data Center, the NCAR's Data Support Section and Atmospheric
688 Chemistry Division, the Latin American Observatory (OLE2), the Sao Paulo
689 Environmental Protection Agency (CETESB), the OpenStreetMap Data Extracts, and
690 the NCAR Command Language (NCL) software for providing the tools and datasets
691 used in this research.

692

693 **6. References**

- 694 Ackermann, I. J., Hass, H., Memmesheimer, M., Ebel, A., Binkowski, F. S., and
695 Shankar, U.: Modal aerosol dynamics model for Europe: development and
696 first applications, *Atmos. Environ.*, 32, 2981-2999, 1998.
- 697 Ahmadov, R., McKeen, S. A., Robinson, A. L., Bahreini, R., Middlebrook, A. M., de
698 Gouw, J. A., Meagher, J., Hsie, E. Y., Edgerton, E., Shaw, S., and Trainer,
699 M.: A volatility basis set model for summertime secondary organic
700 aerosols over the eastern United States in 2006, *Journal of Geophysical*
701 *Research*, 117, D06301, doi:10.1029/2011JD016831, 2012.
- 702 Albuquerque, T. T. A., Andrade, M. F., and Ynoue, R. Y.: Characterization of
703 atmospheric aerosols in the city of Sao Paulo, Brazil: comparisons between
704 polluted and unpolluted periods, *Water Air Soil Pollution*, 195, 201-213, 2011.
- 705 Anderson, L.: Ethanol fuel use in Brazil: air quality impacts, *Energy Environ. Sci.*, 2,
706 1015-1037, 2009.

707 Andrade, M. F., Ynoue, R. Y., Freitas, E. D., Todesco, E., Vara-Vela, A., Ibarra, S.,
708 Martins, L. D., Martins, J. A., Carvalho, V. S. B.: Air quality forecasting system
709 for Southeastern Brazil, *Front. Environ. Sci.*, 3, 1-14, 2015.

710 Andrade, M. F., Fornaro, A., Miranda, R. M., Kerr, A., Oyama, B., Andre, P. A., and
711 Saldiva, P.: Vehicle emissions and PM_{2.5} mass concentrations in six
712 Brazilian cities, *Air Quality, Atmosphere and Health*, 5, 79-88, 2012.

713 Binkowski, F. S. and Shankar, U.: The regional particulate matter model, 1. Mode
714 description and preliminary results, *Journal of Geophysical Research*, 100,
715 26191-26209, 1995.

716 Birch, M. E. and Cary, R. A.: Elemental carbon-based method for occupational
717 monitoring of particulate diesel exhaust: methodology and exposure issues,
718 *Aerosol Science and Technology*, 25, 221-241, 1996.

719 Brito, J., Rizzo, L. V., Herckes, P., Vasconcellos, P. C., Caumo, S. E. S., Fornaro,
720 A., Ynoue, R. Y., Artaxo, P., and Andrade, M. F.: Physical-chemical
721 characterisation of the particulate matter inside two road tunnels in the Sao
722 Paulo Metropolitan Area, *Atmos. Chem. Phys.*, 13, 12199-12213, 2013.

723 Brown, S. G., Lee, T., Roberts, P. T., and Collett, J. L. Jr.: Variations in the OM/OC
724 ratio of urban organic aerosol next to a major roadway, *J. Air & Waste Manag. Assoc.*,
725 63(12), 1422-1433, 2013.

726 Carvalho, V. S. B., Freitas, E. D., Martins, L. D., Martins, J. A., Mazzoli, C. R., and
727 Andrade, M. F.: Air quality status and trends over the Metropolitan Area of
728 Sao Paulo, Brazil as a result of emission control policies, *Environmental*
729 *Science & Policy*, 47, 68-79, 2015.

730 Castanho, A. D. A. and Artaxo, P.: Sao Paulo aerosol source apportionment for
731 wintertime and summertime, *Atmos. Environ.*, 35, 4889-4902, 2001.

732 Costa, R. C. and Sodr , J. R.: Hydrous ethanol vs. gasoline-ethanol blend: Engine
733 performance and emissions, *Fuel*, 89, 287-293, 2010.

734 CETESB-Companhia de Tecnologia de Saneamento Ambiental. Relatorio Anual
735 de Qualidade do Ar no Estado de Sao Paulo 2012, Sao Paulo, 2013.

736 CETESB-Companhia de Tecnologia de Saneamento Ambiental. Emiss es
737 veiculares no Estado de S o Paulo 2011, Sao Paulo, 2012.

738 CETESB-Companhia de Tecnologia de Saneamento Ambiental. Relatorio Anual
739 de Qualidade do Ar no Estado de Sao Paulo 2009, Sao Paulo, 2010.

740 Chang, J. S., Binkowki, F. S., Seaman, N. L., McHenry, J. N., Samson, P. J.,
741 Stockwell, W. R., Walcek, C. J., Madronich, S., Middleton, P. B., Pleim, J. E.,
742 and Lansford, H. H.: The regional acid deposition model and engineering
743 model, State-of-Science/Technology, Report 4, National Acid Precipitation
744 Assessment Program, Washington, DC, 1989.

745 Draxler, R. R. and Hess, G. D.: An overview of the HYSPLIT 4 modelling system of
746 trajectories, dispersion, and deposition, *Aust. Meteor. Mag.*, 47, 295-308, 1998.

747 Emmons, L. K., Walters, S., Hess, P. G., Lamarque, F., Pfister, G. G., Fillmore, D.,
748 Granier, C., Guenther, A., Kinnison, D., Laepple, T., Orlando, J., Tie, X.,
749 Tyndall, G., Wiedinmyer, C., Baughcum, S. L., and Kloster, S.: Description
750 and evaluation of the Model for Ozone and Related chemical Tracers, version
751 4 (MOZART-4), *Geosci. Model Dev.*, 3, 43-67, 2010.

752 Ginoux, P., Chin, M., Tegen, I., Prospero, J. M., Holben, B., Dubovik, O., and Lin,
753 S-J.: Sources and distributions of dust aerosols simulated with the GOCART
754 model, *Journal of Geophysical Research*, 106, 20,255-20,273, 2001.

755 Gong, S. L.: A parameterization of sea-salt aerosol source function for sub- and super-
756 micron particles, *Global Biogeochemical Cycles*, 17, 1097,
757 doi:10.1029/2003GB002079, 2003.

758 Gorin, C. A., Collett, J. L. Jr., and Herckes, P.: Wood smoke contribution to winter
759 aerosol in Fresno, CA, *J. Air & Waste Manag. Assoc.*, 56(11), 1584-1590,
760 2006.

761 GrEC-Grupo de Estudos Climáticos. Relatório climatológico mensal, previsão climática
762 para o Brasil: Set-Out-Nov/2012, Sao Paulo, 2012a. Available at:
763 www.grec.iag.usp.br/link_grec_old/relatorios_climatologicos/2012/agosto/.

764 GrEC-Grupo de Estudos Climáticos. Relatório climatológico mensal, monitoramento
765 climático para o Brasil: Set/2012, Sao Paulo, 2012b. Available at:
766 www.grec.iag.usp.br/link_grec_old/relatorios_climatologicos/2012/setembro/.

767 Grell, G. A., Peckham, S. E., Schmitz, R., McKeen, S. A., Wilczak, J., and Eder, B.:
768 Fully coupled “online” chemistry within the WRF model, *Atmos. Environ.*, 39,
769 6957-6975, 2005.

770 Guenther, A. B., Zimmerman, P. R., Harley, P. C., Monson, R. K., and Fall, R.:
771 Isoprene and monoterpene emission rate variability: model evaluations and
772 sensitivity analyses, *Journal of Geophysical Research*, 98D, 12609-12617,
773 1993.

774 Guenther, A., Zimmerman, P., and Wildermuth, M.: Natural volatile organic
775 compound emission rate estimates for US woodland landscapes, *Atmos.*
776 *Environ.*, 28, 1197-1210, 1994.

777 Fast, J. D., Gustafson, W. I., Easter, R. C., Zaveri, R. A., Barnard, J. C., Chapman,
778 E. G., Grell, G. A., and Peckham, S. E.: Evolution of ozone, particulates, and
779 aerosol direct radiative forcing in the vicinity of Houston using a fully

780 coupled meteorology-chemistry-aerosol module, *Journal of Geophysical*
781 *Research*, 111, D21305, doi:10.1029/2005JD006721, 2006.

782 Forkel, R., Werhahn, J., Hansen, A. B., McKeen, S., Peckham, S., Grell, G., and
783 Suppan, P.: Effect of aerosol-radiation feedback on regional air quality - A
784 case study with WRF/Chem, *Atmospheric Environment*, 53, 202-211, 2012.

785 Heal, M. R., Kumar, P., and Harrison, R. M.: Particles, air quality, policy and health,
786 *Chem. Soc. Rev.*, 41, 6606-6630, 2012.

787 Jenkin, M. E. and Clemitshaw, K. C.: Ozone and other secondary photochemical
788 pollutants: chemical processes governing their formation in the planetary
789 boundary layer, *Atmos. Environ.*, 34, 2499-2527, 2000.

790 Kroll, J. H. and Seinfeld, J. H.: Chemistry of secondary organic aerosol: Formation and
791 evolution of low-volatility organics in the atmosphere, *Atmos. Environ.*, 42,
792 3593-3624, 2008.

793 Kulmala, M., Laaksonen, A., and Pirjola, L.: Parameterization for sulphuric
794 acid/water nucleation rates, *Journal of Geophysical Research*, 103, 8301-
795 8307, 1998.

796 Kumar, P., Morawska, L., Birmili, W., Paasonen, P., Hu, M., Kulmala, M., Harrison,
797 R.M., Norford, L., and Britter, R.: Ultrafine particles in cities, *Environment*
798 *International*, 66, 1-10, 2014.

799 Kumar, P., Robins, A., Vardoulakis, S., and Britter, R.: A review of the characteristics
800 of nanoparticles in the urban atmosphere and the prospects for developing
801 regulatory control, *Atmos. Environ.*, 44, 5035-5052, 2010.

802 Kumar, P., Ketzel, M., Vardoulakis, S., Pirjola, L., Britter, R.: Dynamics and dispersion
803 modelling of nanoparticles from road traffic in the urban atmospheric
804 environment - a review, *J. Aerosol Sci.*, 42, 580-603, 2011.

805 Li, G., Bei, N., Tie, X., and Molina, L. T.: Aerosol effects on the photochemistry in
806 Mexico City during MCMA-2006/MILAGRO campaign, *Atmos. Chem. Phys.*,
807 11, 5169-5182, 2011a.

808 Li, G., Zavala, M., Lei, W., Tsimpidi, A. P., Karydis, V. A., Pandis, S. N.,
809 Canagaratna, M. R., and Molina, L. T.: Simulations of organic aerosol
810 concentrations in Mexico City using the WRF-Chem model during the
811 MCMA-2006/MILAGRO campaign, *Atmos. Chem. Phys.*, 11, 3789-3809,
812 2011b.

813 Li, G., Zhang, R., and Fan, J.: Impacts of black carbon aerosol on photolysis and
814 ozone, *Journal of Geophysical Research*, 110, D23206,
815 doi:10.1029/2005JD005898, 2005.

816 Marple, V. A., Rubow, K. L., Ananth, G. P., and Fissan, H. J.: Micro-Orifice Uniform
817 Deposit Impactor, *Journal of Aerosol Science*, 17, 489-494, 1986.

818 Martins, L. D., Vasconcellos, P. C., Carvalho, L. F., Andrade, M. F.: Estimated impact
819 of biogenic hydrocarbon emissions on photochemical oxidant formation in Sao Paulo
820 during two periods of the winters of 1999-2000, *Revista Brasileira de Meteorologia*, 21,
821 190-200, 2006.

822 McMurry, P., Shepherd, M., and Vickery, J.: *Particulate Matter Science for Policy*
823 *Makers: A NARSTO Assessment*, Cambridge University Press, Cambridge,
824 England, 2004.

825 Middleton, P., Stockwell, W. R., and Carter, W. P. L.: Aggregation and analysis of
826 volatile organic compound emissions for regional modelling, *Atmos.*
827 *Environ.*, 24A, 1107-1133, 1990.

828 Miranda, R. M. and Andrade, M. F.: Physicochemical characteristics of atmospheric
829 aerosols during winter in the Sao Paulo Metropolitan Area in Brazil, *Atmos.*
830 *Environ.*, 39, 6188-6193, 2005.

831 Monahan, E. C., Spiel, D. E., Davidson, K. L.: A model of marine aerosol generation
832 via whitecaps and wave disruption. In: Monahan, E. C., MacNiocaill, G. D.
833 (Eds.), *Oceanic Whitecaps*. Reidel Publishing Company, Norwell, Mass, 167-
834 174, 1986.

835 Muñoz, A. G., López, P., Velásquez, R., Monterrey, L., León, G., Ruiz, F., Recalde,
836 C., Cadena, J., Mejía, R., Paredes, M., Bazo, J., Reyes, C., Carrasco, G.,
837 Castellón, Y., Villarroel, C., Quintana, J., and Urdaneta, A.: An
838 Environmental Watch System for the Andean Countries: El Observatorio
839 Andino, *Bull. Amer. Meteor. Soc.*, 91, 1645-1652, 2010.

840 Muñoz, A. G., Ruiz-Carrascal, D., Ramírez, P., León, G., Quintana, J., Bonilla, A.,
841 Torres, W., Pastén, M., and Sánchez, O.: Risk Management at the Latin
842 American Observatory, in: *Risk Management—Current Issues and Challenges*,
843 InTech Publications, doi:10.5772/50788, 533-556, 2012.

844 Nogueira, T., Dominutti, P. A., De Carvalho, L. R. F., Fornaro, A., and Andrade, M.
845 F.: Formaldehyde and acetaldehyde measurements in urban atmosphere
846 impacted by the use of ethanol biofuel: Metropolitan Area of Sao Paulo, 2012-
847 2013, *Fuel*, 134, 505-513, 2014.

848 Odum, J. R., Hoffmann, T., Bowman, F., Collins, D., Flagan, R. C., and Seinfeld, J.
849 H.: Gas/particle partitioning and secondary organic aerosol yields,
850 *Environmental Science Technology*, 30, 2580-2585, 1996.

851 Pankow, J. F.: An absorption model of the gas aerosol partitioning involved in the
852 formation of secondary organic aerosol, *Atmos. Environ.*, 28, 185-188, 1994a.

853 Pankow, J. F.: An absorption model of the gas aerosol partitioning involved in the
854 formation of secondary organic aerosol, *Atmos. Environ.*, 28, 189-93, 1994b.

855 Pérez-Martínez, P. J., Andrade, M. F., and Miranda, R. M.: Traffic-related air quality
856 trends in Sao Paulo, Brazil, *J. Geophys. Res. Atmos.*, 120, 6290-6304,
857 doi:10.1002/2014JD022812, 2015.

858 Pérez-Martínez, P. J., Miranda, R. M., Nogueira, T., Guardani, M. L., Fornaro, A.,
859 Ynoue, R., and Andrade, M. F.: Emission factors of air pollutants from
860 vehicles measured inside road tunnels in Sao Paulo: case study comparison,
861 *Int. J. Environ. Sci. Technol.*, 11, 2155-2168, 2014.

862 Real, E. and Sartelet, K.: Modelling of photolysis rates over Europe: impact on
863 chemical gaseous species and aerosols, *Atmos. Chem. Phys.*, 11, 1711-1727,
864 2011.

865 Salvo, A. and Geiger, F. M.: Reduction in local ozone levels in urban Sao Paulo due to
866 a shift from ethanol to gasoline use, *Nature Geoscience*, 7, 450-458,
867 doi:10.1038/ngeo2144, 2014.

868 Saxena, P., Hudischewskyj, A. B., Seigneur, C., and Seinfeld, J. H.: A comparative
869 study of equilibrium approaches to the chemical characterization of
870 secondary aerosols, *Atmos. Environ.*, 20, 1471-1483, 1986.

871 Schell, B., Ackerman, I. J., Hass, H., Binkowski, F. S., and Ebel, A.: Modelling the
872 formation of secondary organic aerosol within a comprehensive air quality
873 model system, *Journal of Geophysical Research*, 106, 28275-28293, 2001.

874 Seinfeld, J. H. and Pandis, S. N.: *Atmospheric Chemistry and Physics: from air
875 pollution to climate change*, Second Edition, Jhon Wiley, New Jersey,
876 2006.

877 Shrivastava, M., Berg, L. K., Fast, J. F., Easter, R. C., Laskin, A., Chapman, E. G.,
878 Gustafson Jr, W. I., Liu, Y., and Berkowitz, C. M.: Modelling aerosols and
879 their interactions with shallow cumuli during the 2007 CHAPS field study,
880 Journal of Geophysical Research: Atmospheres, 118, 1343-1360, 2013.

881 Taylor, K. E.: Summarizing multiple aspects of model performance in a single diagram,
882 Journal of Geophysical Research, 106(D7), 7183-7192,
883 doi:10.1029/2000JD900719, 2001.

884 Tuccella, P., Curci, G., Visconti, G., Bessagnet, B., Menut, L., and Park, R. J.:
885 Modelling of gas and aerosol with WRF-Chem over Europe: Evaluation and
886 sensitivity study, Journal of Geophysical Research, 117, D03303,
887 doi:10.1029/2011JD016302, 2012.

888 Vasconcellos, P. C., Souza, D. Z., Sanchez-Ccoyllo, O. R., Bustillos, J. O. V., Lee,
889 H., Santos, F. C., Nascimento, K. H., Araujo, M. P., Saarnio, K., Teinila, K.,
890 and Hillamo, R.: Determination of anthropogenic and biogenic
891 compounds on atmospheric aerosol collected in urban, biomass burning
892 and forest areas in Sao Paulo, Brazil, Science of the Total Environment, 408,
893 5836-5844, 2010.

894 Vieira-Filho, M. S., Pedrotti, J. J., and Fornaro, A.: Contribution of long and mid-range
895 transport on the sodium and potassium concentrations in rainwater samples, Sao
896 Paulo megacity, Brazil, Atmos. Environ., 79, 299-307, 2013.

897 Wedding, J. B., Weigand, M., John, W., and Wall, S.: Sampling effectiveness of the
898 inlet to the dichotomous sampler, Environ. Sci. Technol., 14(11), 1367-1370,
899 1980.

900 Ynoue, R. Y. and Andrade, M. F.: Size-resolved mass balance of aerosol particles over
901 the Sao Paulo Metropolitan Area of Brazil, *Aerosol Science and Technology*, 1,
902 52-62, 2004.

903 Table 1. Description of aerosol sampling campaigns performed at IAG-USP.

Parameter	Sampling frequency	Period of sampling	Sampling device
Aerosol mass size distribution	24 hours	July-September	MOUDI impactor
PM _{2.5} and PM ₁₀ concentration	12 hours	July-September	Dichotomous sampler
OC and EC concentration	12 hours	August-September	Sunset OC-EC analyser

904

905

906 Table 2. Description of measurement sites.

Site	Initials	Latitude	Longitude	Classification	Measured species
Nossa S. do Santana	NSO	-23.4796	-46.6916	Urban	PM ₁₀ , O ₃
Parque D. Mooca	PDP	-23.5448	-46.6276	Urban	PM ₁₀ , O ₃
Cerqueira IAG-USP	MOO	-23.5497	-46.5984	Urban	PM ₁₀ , O ₃
	CCE	-23.5531	-46.6723	Urban	PM ₁₀
	IAG-USP	-23.5590	-46.7330	Suburban	PM ₁₀ , PM _{2.5} , OC, EC, aerosol mass size distrib. ^a
IPEN-USP	IPEN-USP	-23.5662	-46.7374	Suburban	PM _{2.5} , O ₃ , NO _x , CO
Ibirapuera	IBI	-23.5914	-46.6602	Suburban	PM ₁₀ , O ₃ , NO _x , CO
Congonhas	CON	-23.6159	-46.6630	Urban	PM ₁₀ , PM _{2.5}
AF-IAG	AF-IAG	-23.6500	-46.6167	Suburban	T, RH, WS, WD ^b
Santo	SAM	-23.6545	-46.7095	Urban	PM ₁₀
Interlagos	INT	-23.6805	-46.6750	Urban	PM ₁₀ , O ₃ , T, RH, WS, WD

907 ^aincludes SO₄²⁻, NO₃⁻, NH₄⁺, Na⁺, Cl⁻ and PM₁₀.

908 ^bT, RH, WS, and WD denote temperature, relative humidity, wind speed and wind
 909 direction, respectively.

910

911 Table 3. Selected WRF-Chem configuration options.

Atmospheric Process	WRF-Chem option
Longwave radiation	RRTM
Shortwave radiation	Goddard
Surface layer	Monin-Obukhov
Land surface	Noah
Boundary layer	YSU
Cumulus clouds ^a	Grell 3D
Cloud microphysics	Lin
Gas-phase chemistry	RADM2
Aerosol chemistry	MADE/SORGAM
Photolysis	Fast-J

912 ^aOuter domains only

913

914 Table 4. Description of WRF-Chem simulations.

Label	Description
Case_0 (Baseline simulation)	Emission of gases Emission of aerosols Aerosol-radiation feedback turned on
Case_1	Emission of gases No emission of aerosols Aerosol-radiation feedback turned on
Case_2	Emission of gases Emission of aerosols Aerosol-radiation feedback turned off

915

916

917 Table 5. Performance statistics for WRF-Chem predictions at all sites^a

Index	PM _{2.5}	PM ₁₀	O ₃	NO _x	CO	T	RH	WS	WD
MB	-8.84	-14.10	-0.85	-8.75	-0.27	0.65	-5.74	0.54	31.12
MFB (%)	-47.62	-38.19	22.63	12.68	-32.53	1.94	-7.95	41.21	31.66
MFE (%)	47.90	39.90	72.85	82.82	80.93	14.16	23.84	71.12	54.40
RMSE _{UB}	6.83	10.59	27.45	30.35	0.57	3.21	20.06	1.08	79.38
R	0.73	0.72	0.63	0.42	0.54	0.71	0.62	0.41	0.43

918 ^aValues are averaged from all the individual indexes found at the measurement sites.

919 Individual indexes are calculated from both hourly observed and predicted values.

920 Figure 1. Downtown area of the 3 km modelling domain (d03) showing the locations of
921 measurement sites and WRF topography in the vicinity of the SPMA. Red dots
922 represent sites with information on O₃ and PM. Yellow dots represent only
923 sites with information on PM. Blue dot represents the location of the IAG-USP's
924 climatological station.

925 Figure 2. Emission rates for Aromatic VOCs at 19 UTC in the 3 km modelling
926 domain.

927 Figure 3. Hourly accumulated precipitation and relative humidity observed at the
928 IAG-USP's climatological station during the study period.

929 Figure 4. HYSPLIT three-day backward trajectories and locations of fires in Sao Paulo
930 State and part of central-west region of Brazil. Pink markers represent the
931 observed fire locations during the study period considering different satellite
932 products (GOES, AQUA, TERRA, NOAA). The backward trajectories starting
933 at IAG-USP were calculated for the days 9 and 31 August and 5 September 2012
934 at three different altitudes: 500 m (red lines), 1000 m (blue lines), and 2000 m
935 (green lines).

936 Figure 5. Daily (top), diurnal (bottom), and nocturnal (middle) mean concentrations for
937 EC, OC, PM₁₀, PM_{2.5-10}, PM_{2.5} (left panels), and Na, Fe₂SO₃, SiO₂, K₂O, and S
938 (right panels). The PM_{2.5-10} aerosol variable is defined as particulate matter with
939 aerodynamic diameter between 2.5 and 10 µm. The grey line indicates the WHO
940 air quality standard for PM_{2.5} (25 µg m⁻³).

941 Figure 6. The predicted average of wind vectors at 10 m and temperature at 2 m from
942 the baseline simulation (Case_0) for the whole study period in the 3 km
943 modelling domain. Blue dots represent the locations of the measurement sites,

944 whereas cyan numbers represent the observed average temperature in those
945 sites: 17.7 °C in AF-IAG and 17.8 °C in INT.

946 Figure 7. The observed and predicted daily variations of PM_{2.5} concentrations at three
947 sites in SPMA for the 3 km modelling domain.

948 Figure 8. The observed and predicted daily variations of PM₁₀ concentrations at ten sites
949 in SPMA for the 3 km modelling domain.

950 Figure 9. The observed and predicted hourly variations of O₃ concentrations at six sites
951 in SPMA for the 3 km modelling domain.

952 Figure 10. Taylor diagram (Taylor, 2001) showing the individual correlation
953 coefficients, mean biases, and normalized standard deviations for the PM₁₀, PM_{2.5}, OC
954 and EC concentrations.

955 Figure 11. The predicted average surface distribution of PM_{2.5} concentrations for the
956 whole study period in the 3 km modelling domain. Red dots represent the
957 locations of the measurement sites with information on PM_{2.5}, whereas cyan
958 numbers represent the observed average PM_{2.5} concentration in those sites: 23.4
959 μg m⁻³ in IPEN-USP, 21.3 μg m⁻³ in IAG-USP, and 22.2 μg m⁻³ in CON.

960 Figure 12. The predicted average surface distribution of PM₁₀ concentrations for the
961 whole study period in the 3 km modelling domain. Red dots represent the
962 locations of the measurement sites with information on PM₁₀, whereas cyan
963 numbers represent the observed average PM₁₀ concentration in those sites: 49.5
964 μg m⁻³ in IAG-USP and 38.7 μg m⁻³ in CON.

965 Figure 13. The predicted average surface distribution of the PM_{2.5}:PM₁₀ ratio for the
966 whole study period in the 3 km modelling domain. Red dots represent the
967 locations of the measurement sites with information on both PM_{2.5} and PM₁₀,

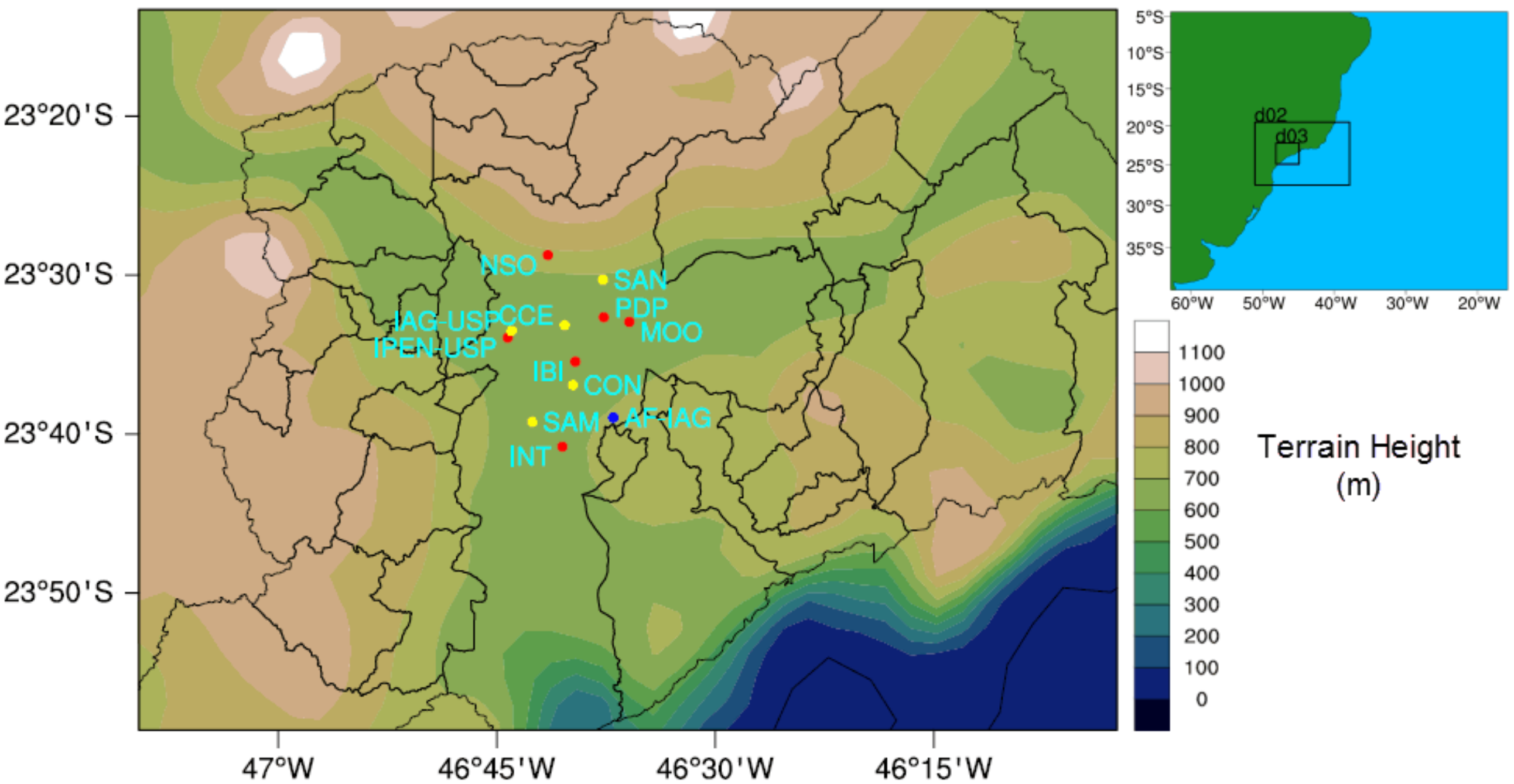
968 whereas cyan numbers represent the observed average $PM_{2.5}:PM_{10}$ ratio in those
969 sites: 0.43 in IAG-USP and 0.57 in CON.

970 Figure 14. The observed and predicted daily variations of OC and EC concentrations
971 at IAG-USP.

972 Figure 15. The observed and predicted average aerosol mass size distribution for SO_4 ,
973 NO_3 , NH_4 , Na, Cl, and other PM_{10} constituents at IAG-USP. The observed
974 aerosol distributions were collected in ten size classes using a rotated impactor
975 (MOUDI) and joined adequately according to the three modes used by the
976 MADE aerosol scheme: Aitken ($<0.1 \mu m$), accumulation ($0.1-1 \mu m$) and coarse
977 ($>1 \mu m$). The five inorganic ions carried in MADE are only calculated for the
978 Aitken and accumulation modes. The WRF's PM_{10} aerosol variable does not
979 include neither OC nor EC for this comparison.

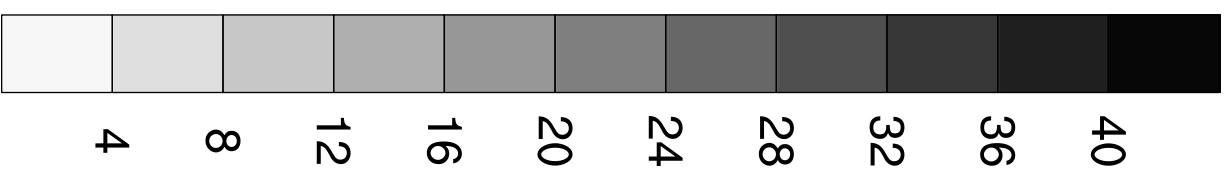
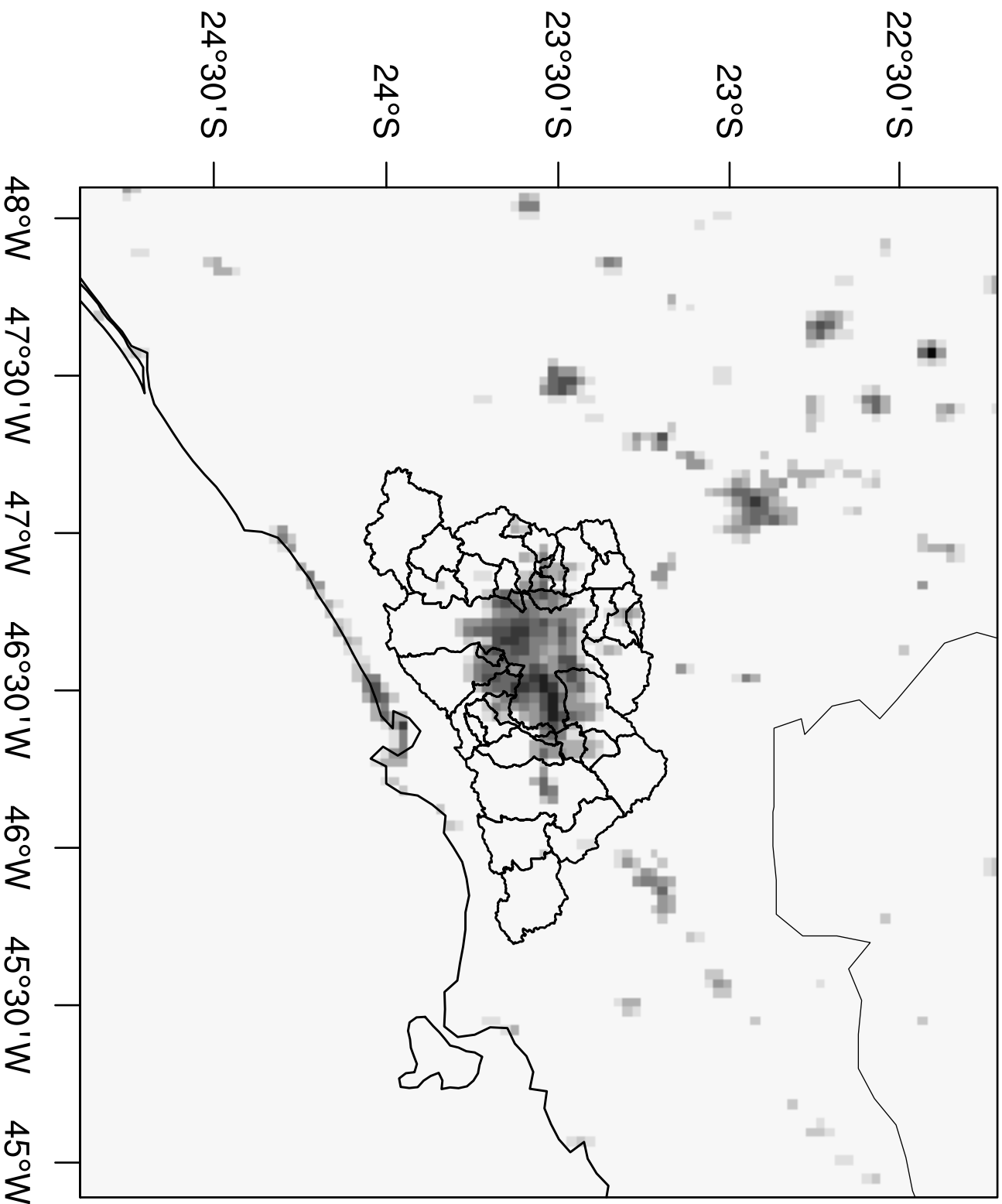
980 Figure 16. The observed and predicted average contributions for the main identified
981 constituents of $PM_{2.5}$ at IAG-USP.

982 Figure 17. The impact of (a) emissions of primary gases on the fine particles formation,
983 (b) emissions of dust-sea salt aerosols on the PM_{10} concentration, and (c) aerosol
984 direct effect on the ground level O_3 concentrations at 16:00 h (local time).

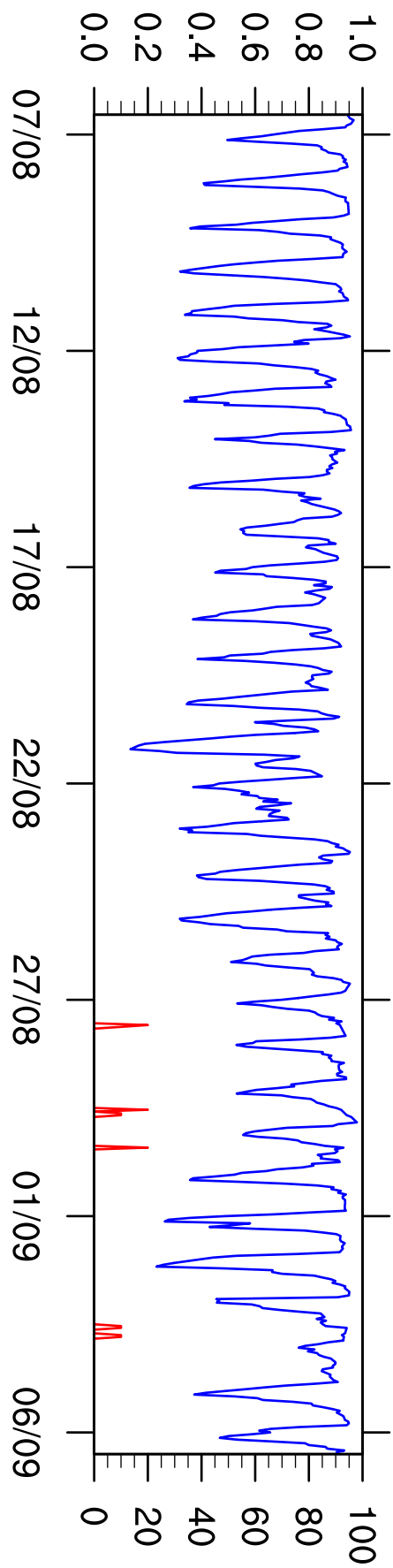


19 UTC

E_TOL (mol/km²/hr)



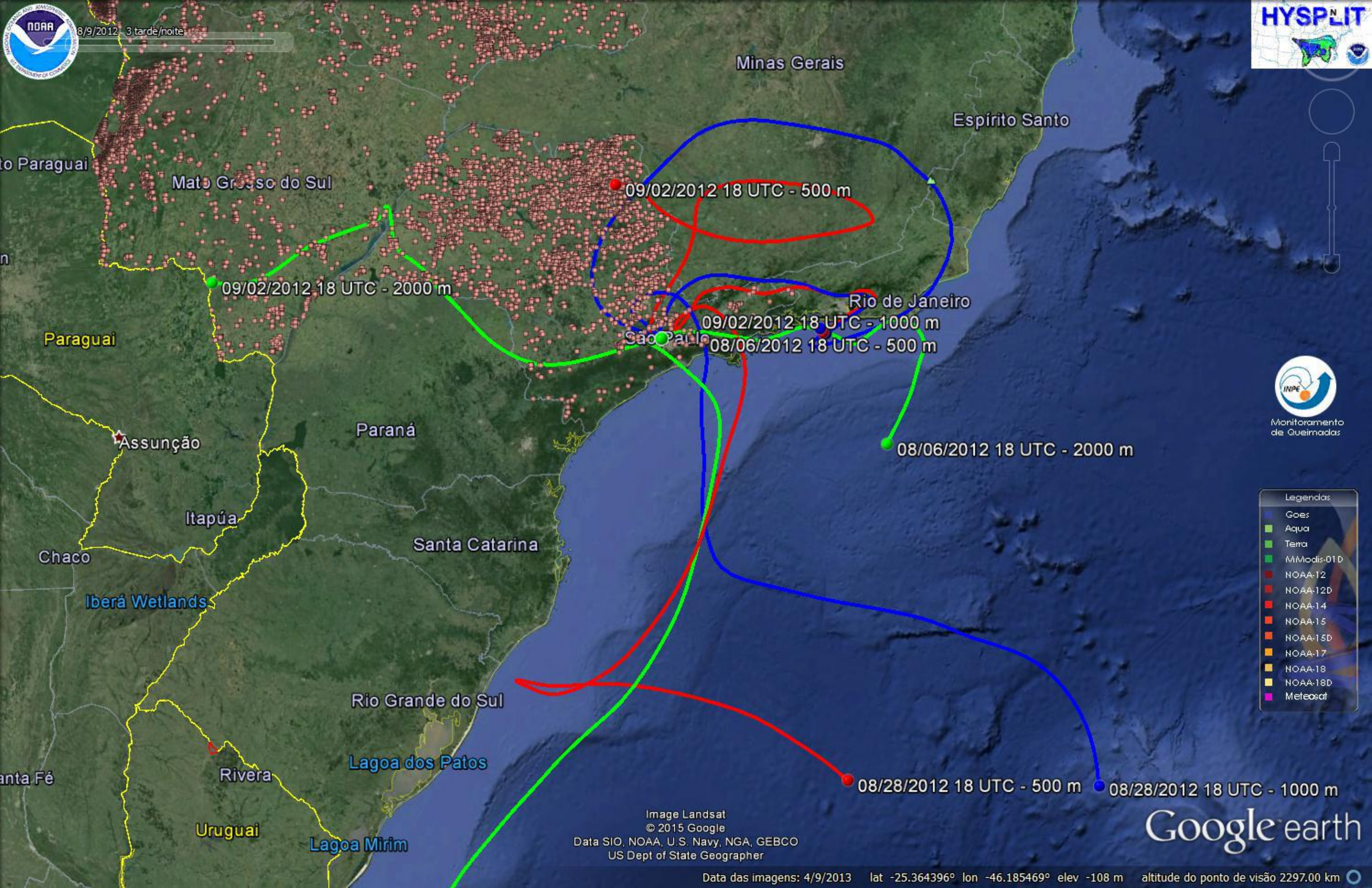
Precipitation (mm) [red]



Humidity (%) [blue]



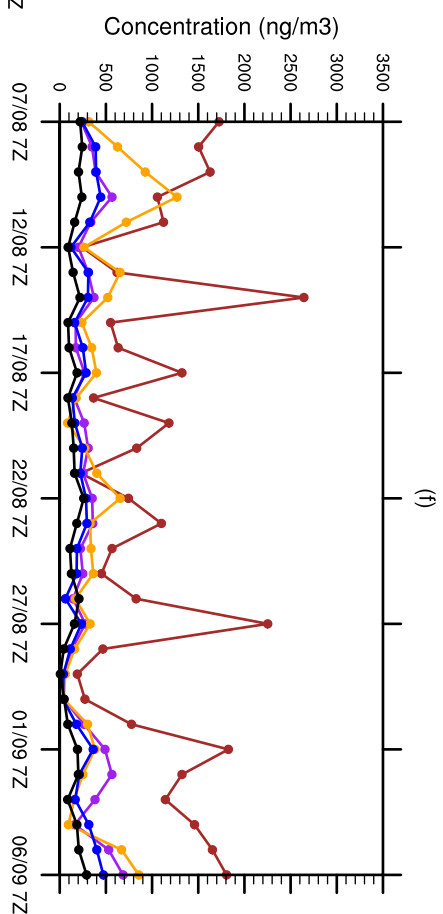
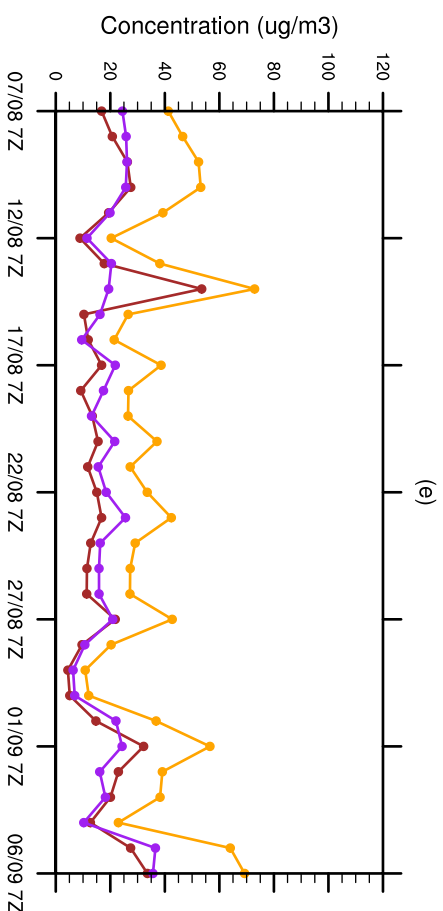
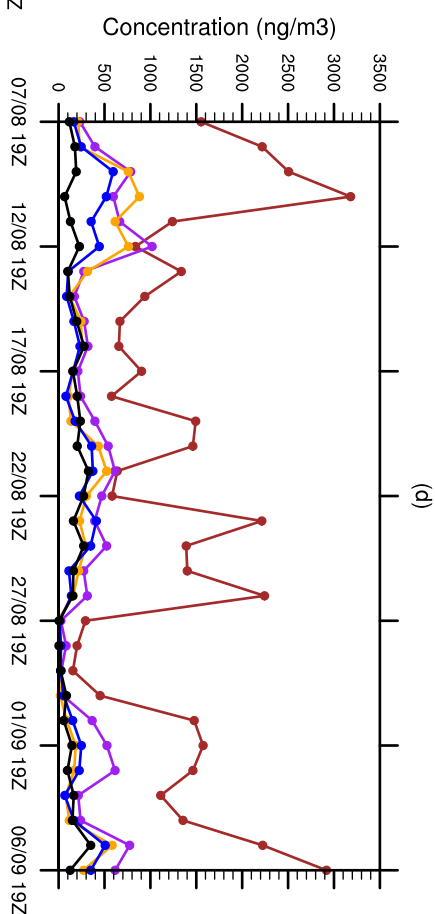
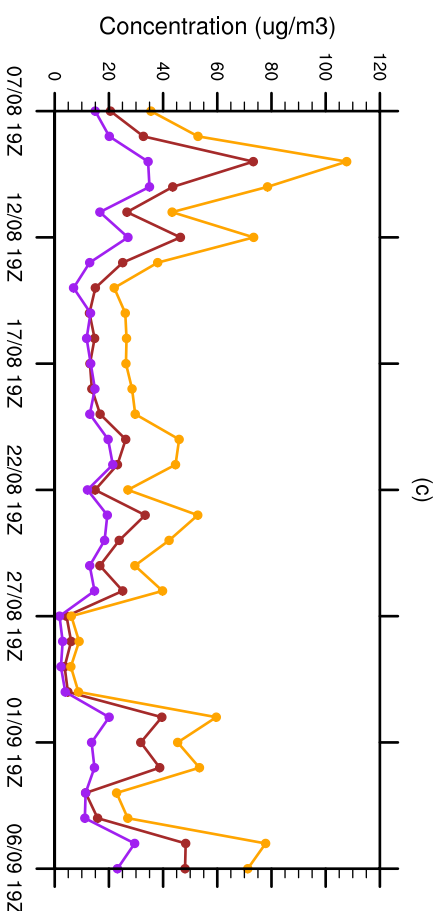
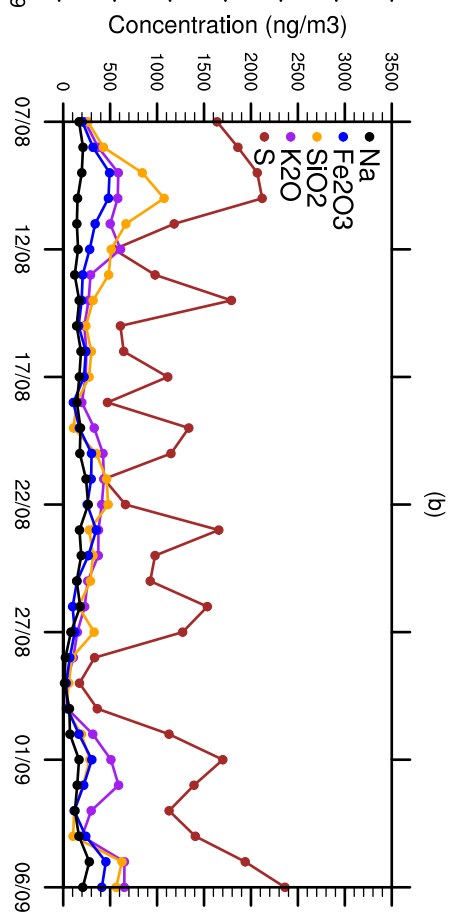
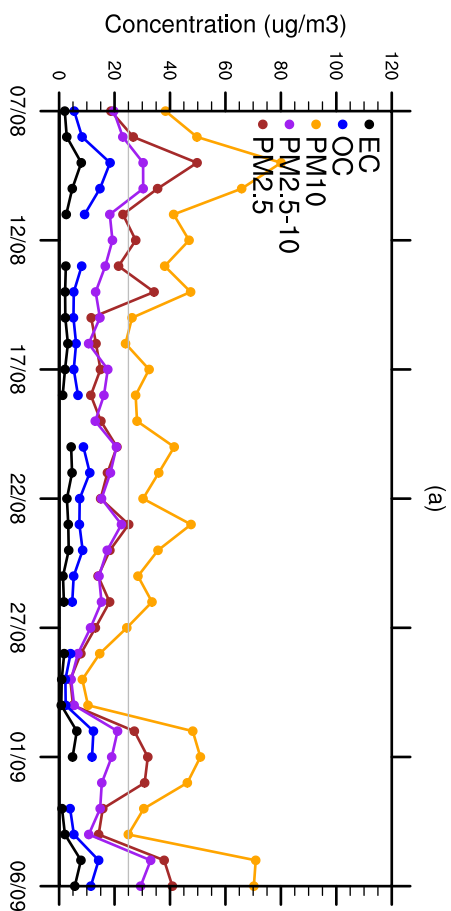
8/9/2012 3 tarde/noite



- Legendas
- Goes
 - Agua
 - Terra
 - MModis-01D
 - NOAA-12
 - NOAA-12D
 - NOAA-14
 - NOAA-15
 - NOAA-15D
 - NOAA-17
 - NOAA-18
 - NOAA-18D
 - Meteosat

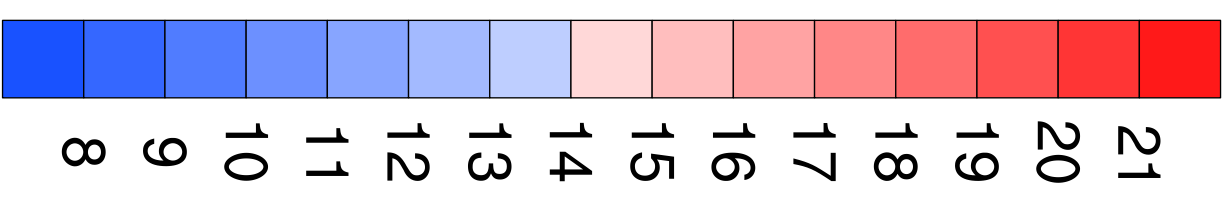
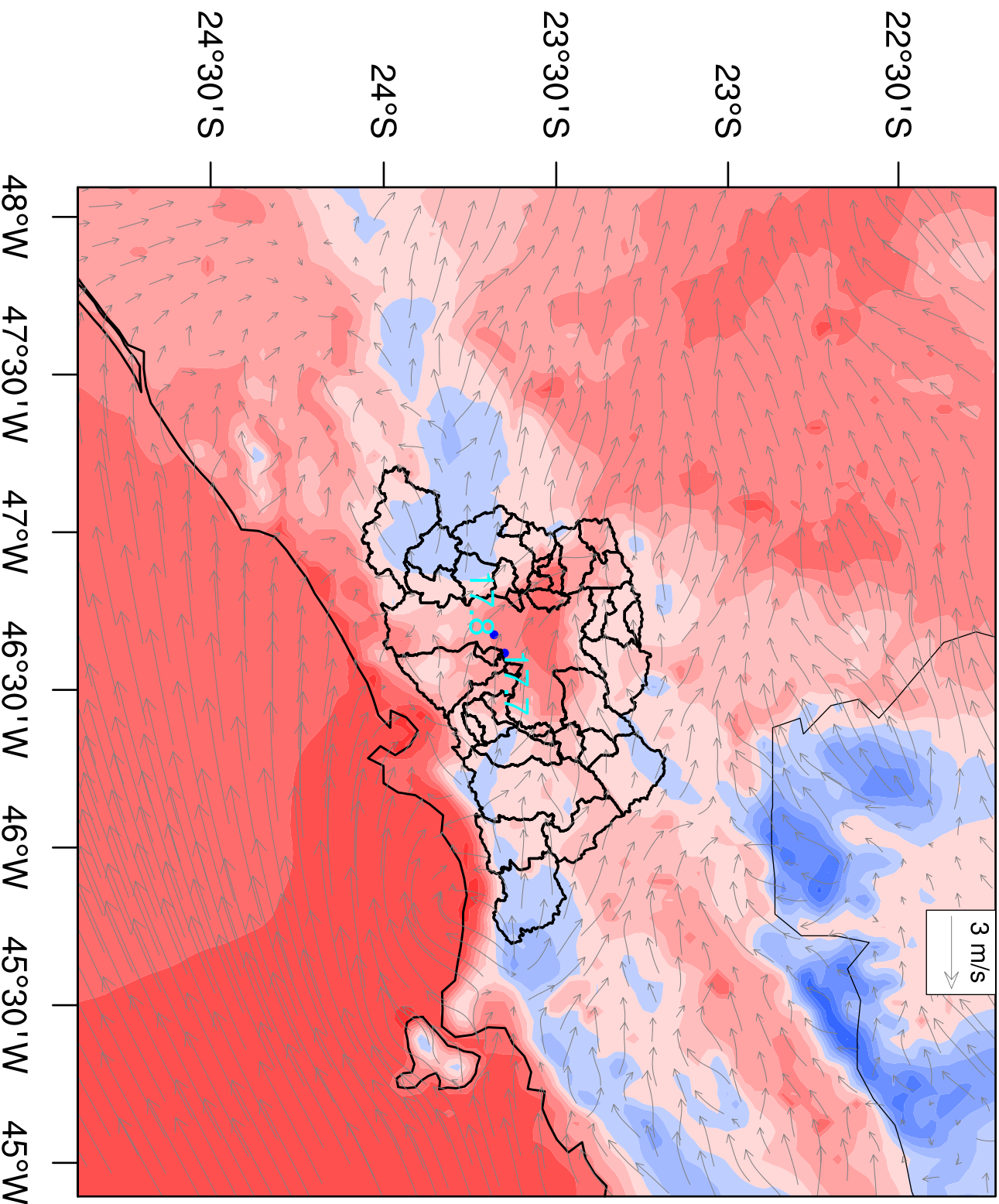
Image Landsat
 © 2015 Google
 Data SIO, NOAA, U.S. Navy, NGA, GEBCO
 US Dept of State Geographer

Google earth

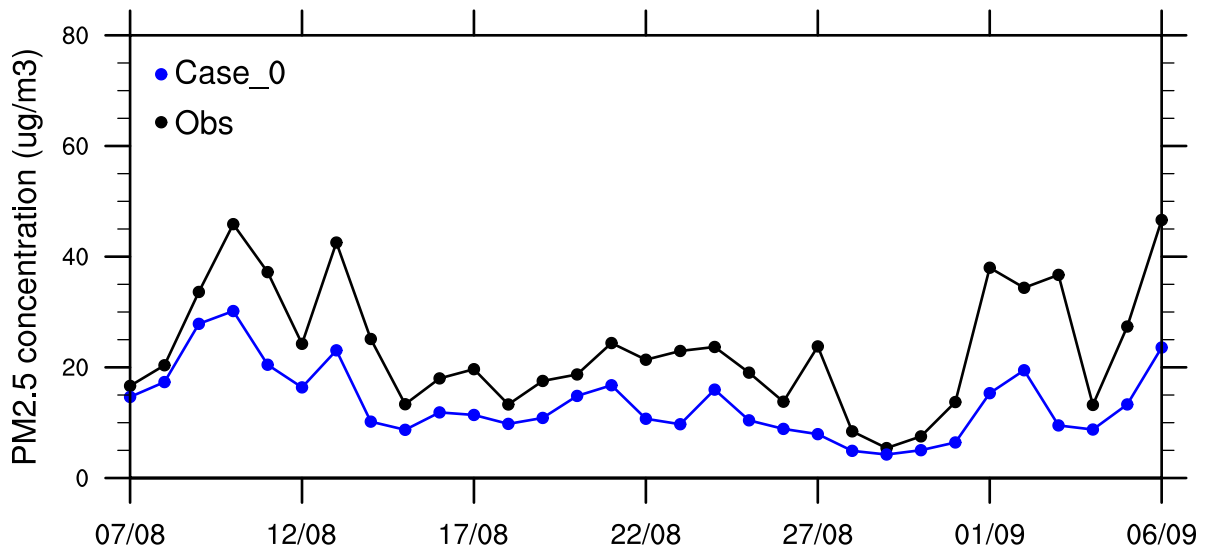


Temperature at 2m (Case_0)

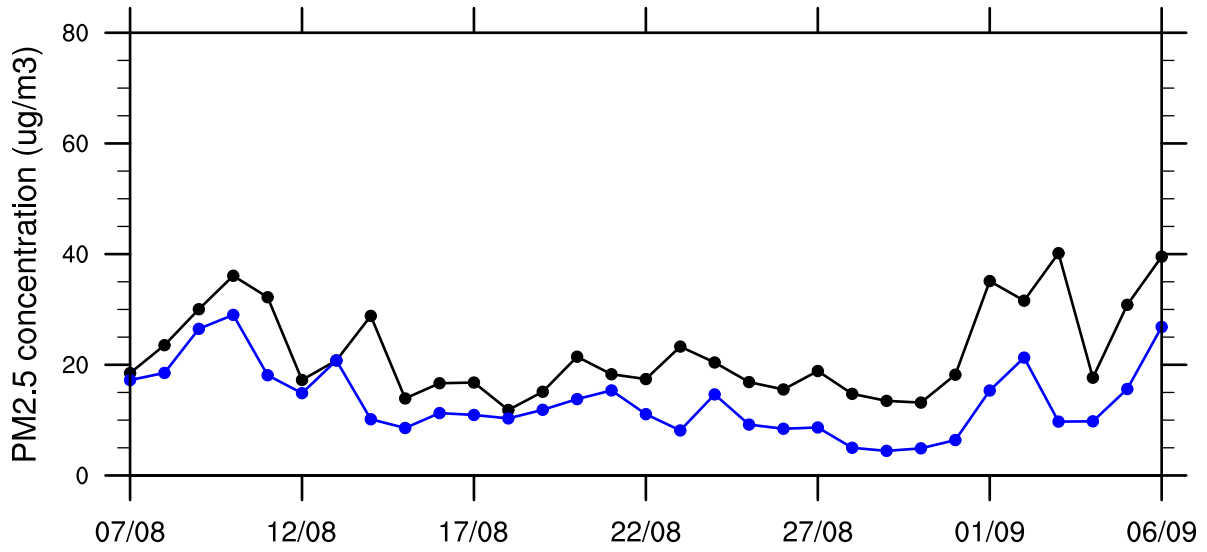
degrees C



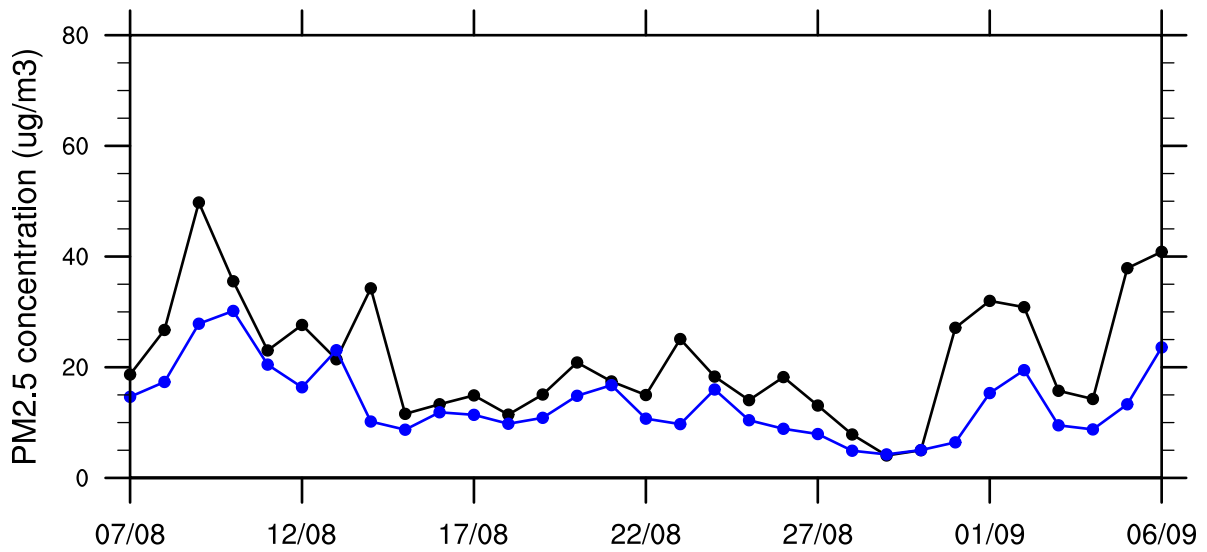
IPEN-USP

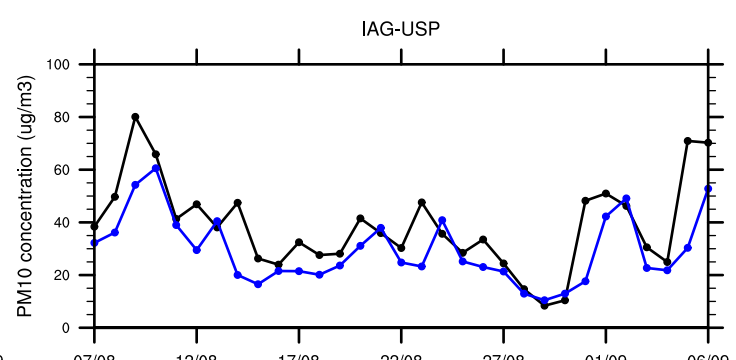
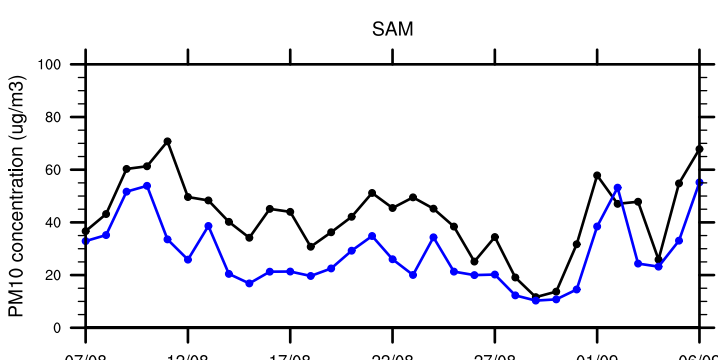
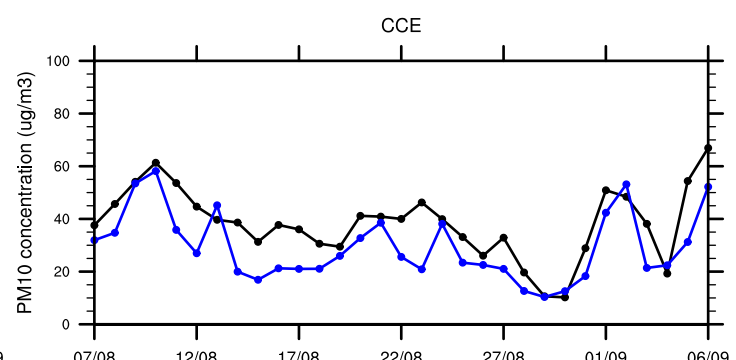
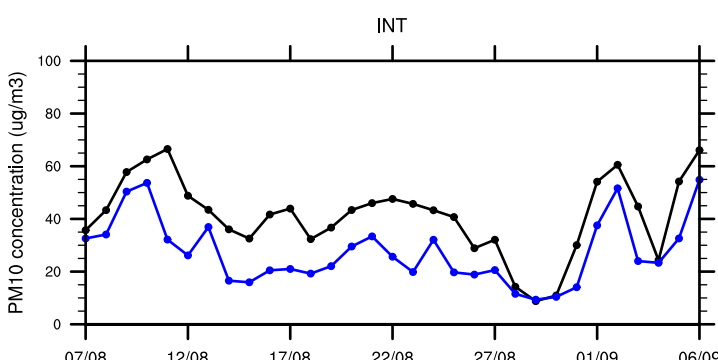
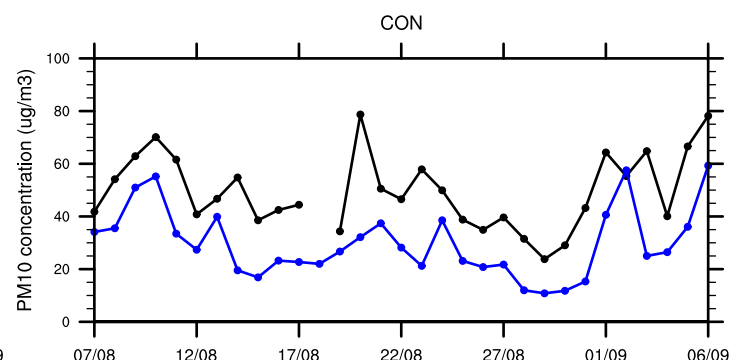
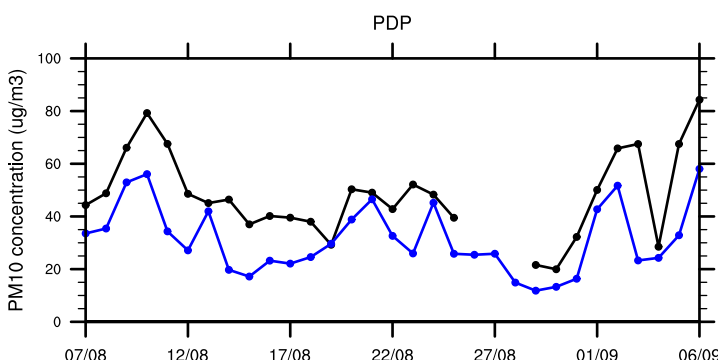
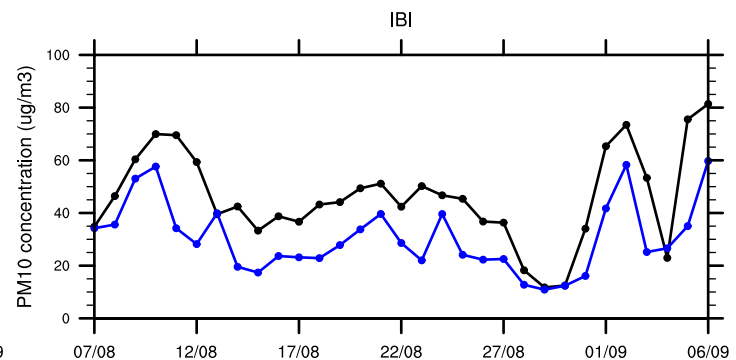
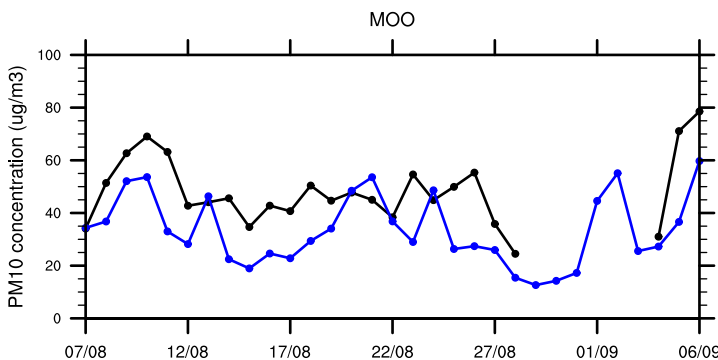
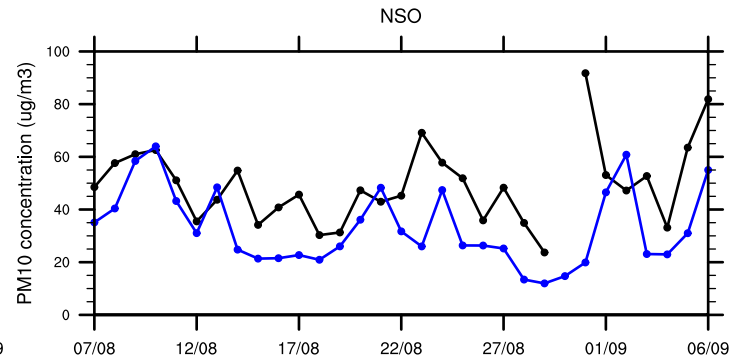
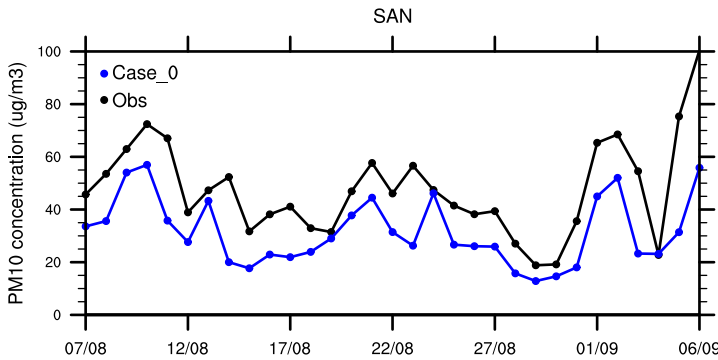


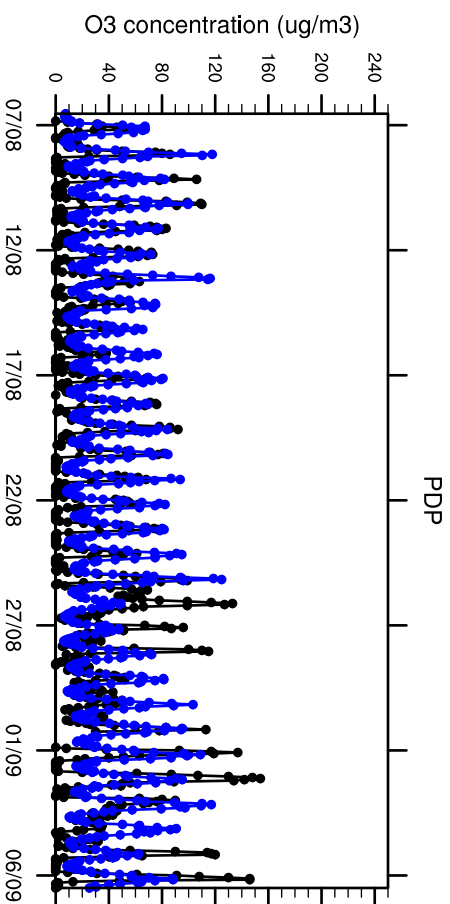
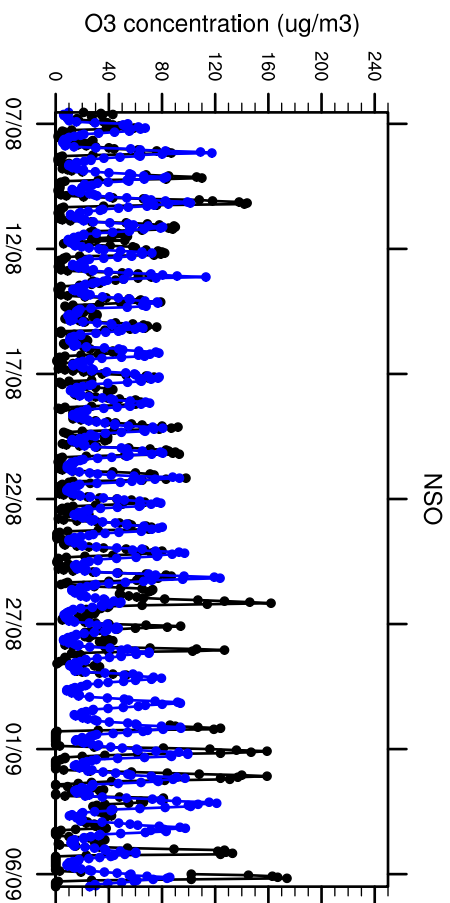
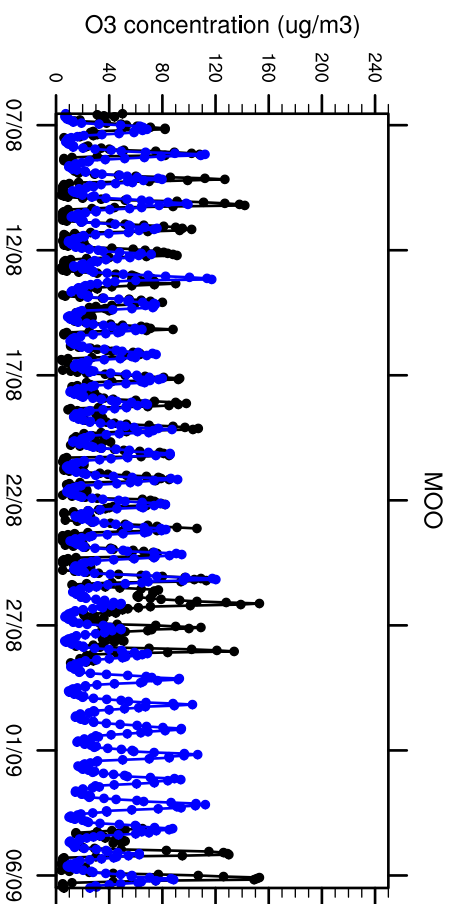
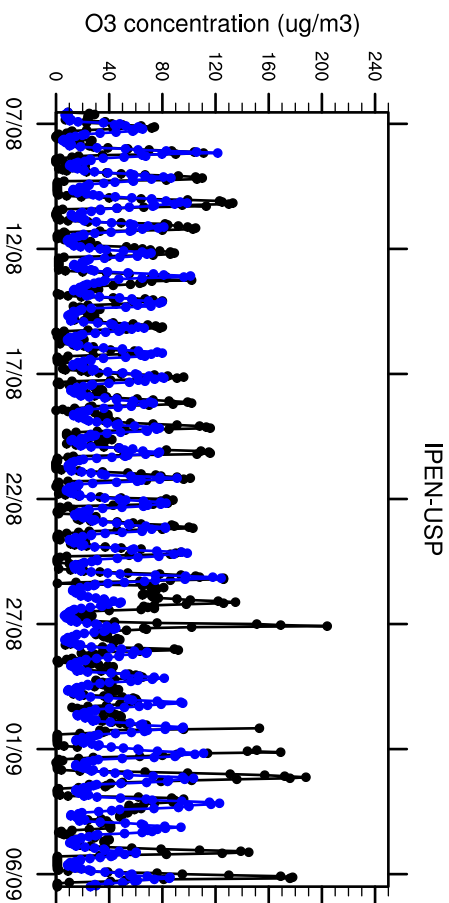
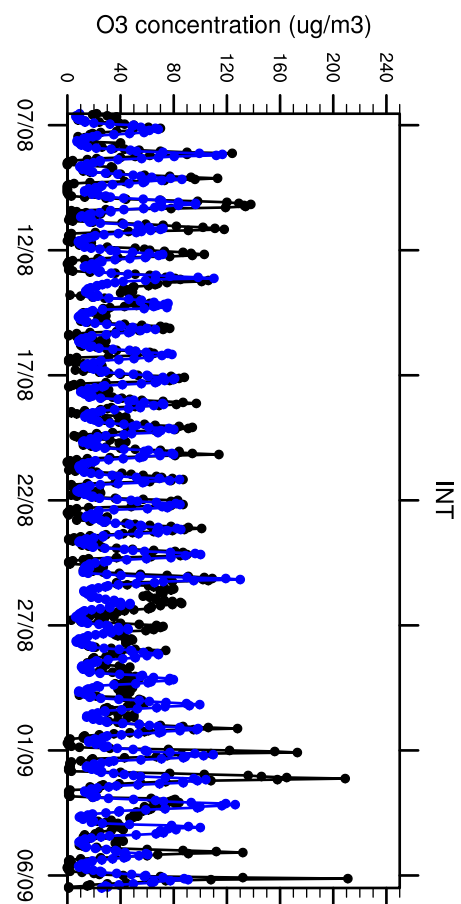
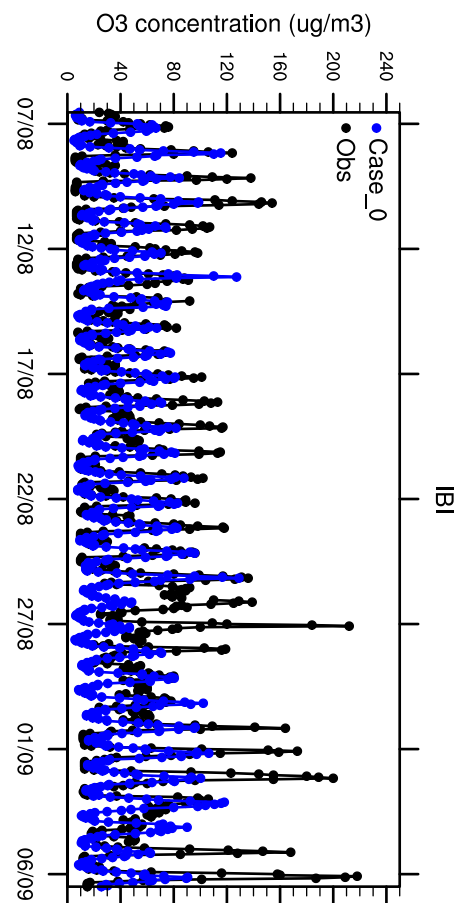
CON

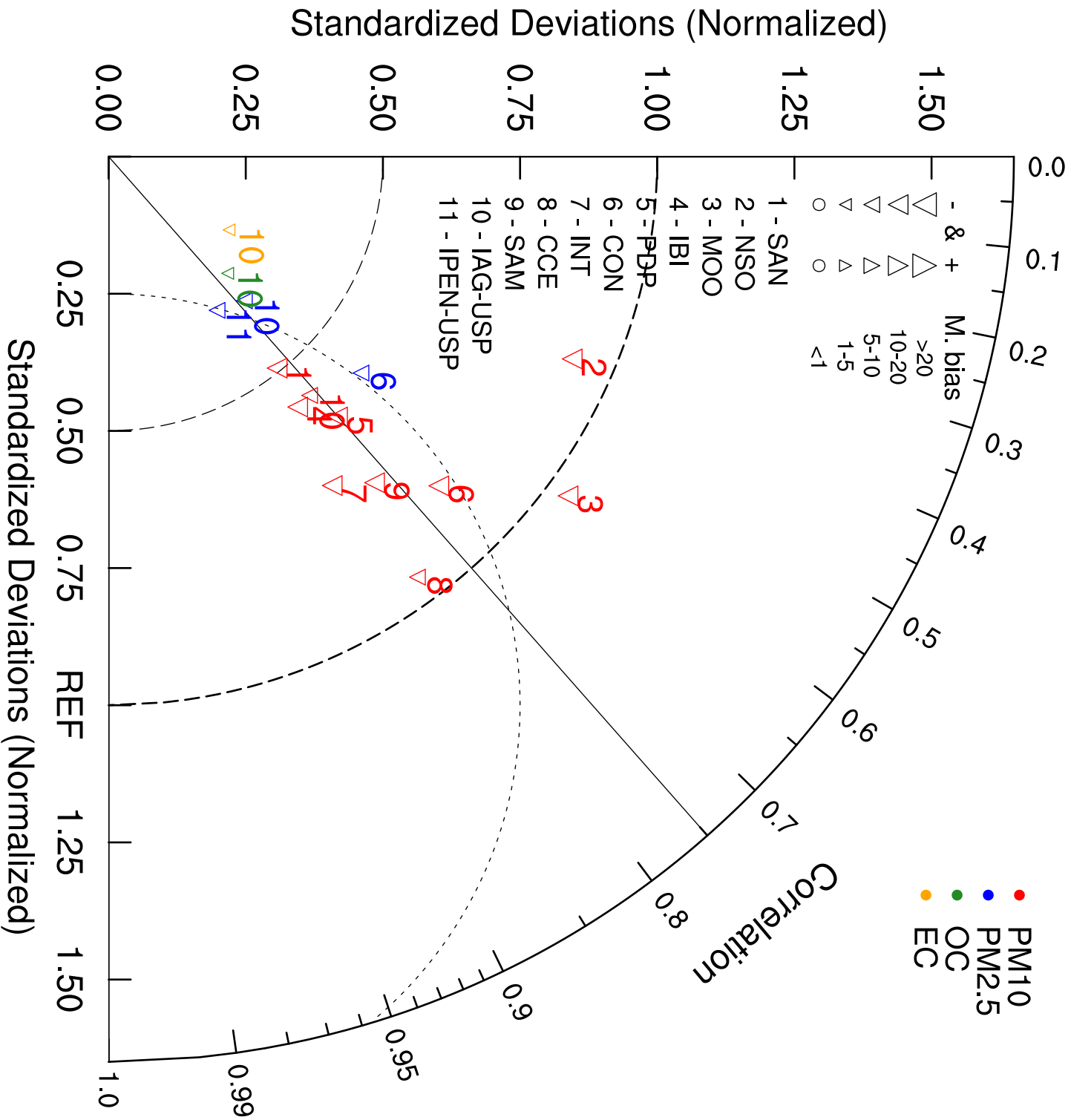


IAG-USP



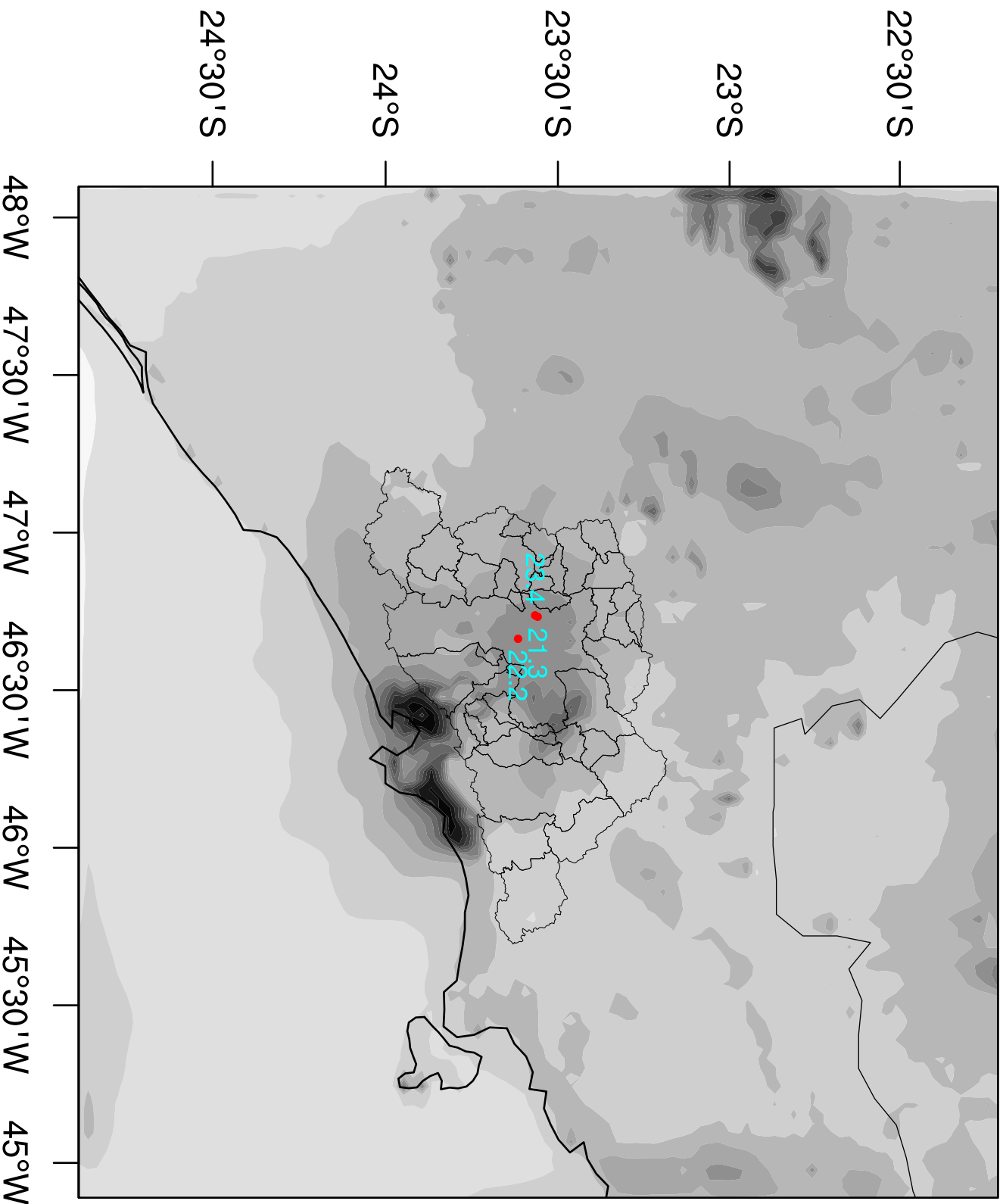






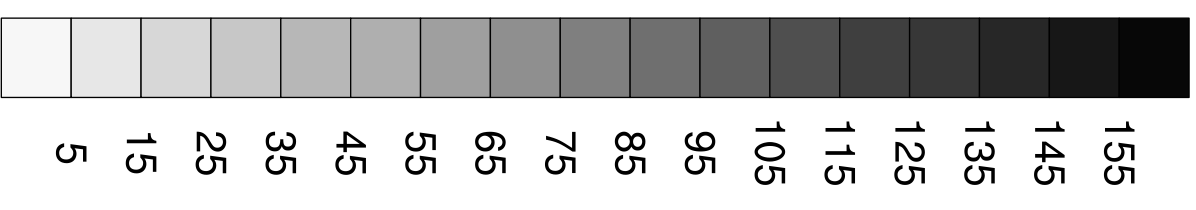
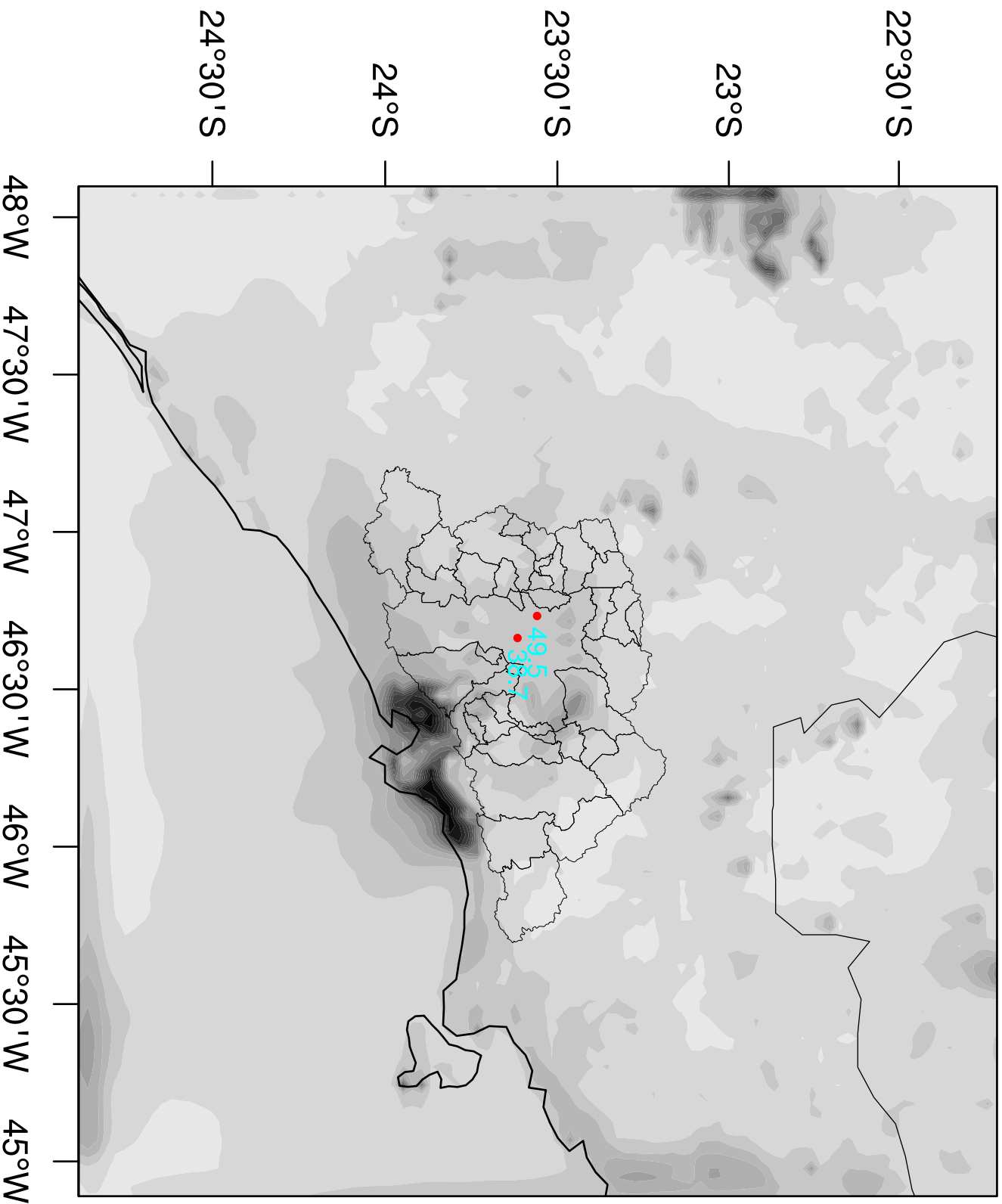
PM2.5 (Case_0)

ug/m3



PM10 (Case_0)

ug/m3



PM2.5 / PM10 (Case_0)

